^{59}Co NMR evidence for charge and orbital order in the kagome-like structure of $Na_{2/3}CoO_2$

I. R. Mukhamedshin[1,2,*] and H. Alloul[1]

[1]*Laboratoire de Physique des Solides, UMR 8502, Université Paris-Sud, FR-91405 Orsay, France, EU*

[2]*Institute of Physics, Kazan University, RU-420008 Kazan, Russia*

(Received 19 July 2011; revised manuscript received 5 September 2011; published 13 October 2011)

We report a complete set of ^{59}Co NMR data taken on the $x = 2/3$ phase of sodium cobaltates Na_xCoO_2 for which we have formerly established the in-plane Na ordering and its three-dimensional stacking from a combination of symmetry arguments taken from Na and Co NQR/NMR data. Here, we resolve all the parameters of the Zeeman and quadrupolar Hamiltonians for all cobalt sites in the unit cell and report the temperature dependencies of the NMR shift and spin lattice relaxation T_1 data for these sites. We confirm that three nonmagnetic Co^{3+} (Co1) are in axially symmetric positions and that the doped holes are delocalized on the nine complementary magnetic cobalt sites (Co2) of the atomic unit cell. The moderately complicated atomic structure resumes then in a very simple electronic structure in which the electrons delocalize on the Co2 kagome sublattice of the triangular lattice of Co sites. The observation of a single temperature dependence of the spin susceptibilities indicates that a single band picture applies, and that the magnetic properties are dominated by the static and dynamic electronic properties at the Co2 sites. We evidence that they display a strong in-plane electronic anisotropy initially unexpected but which agrees perfectly with an orbital ordering along the kagome sublattice organization. These detailed data should now permit realistic calculations of the electronic properties of this compound in order to determine the incidence of electronic correlations.

DOI: 10.1103/PhysRevB.84.155112 PACS number(s): 76.60.−k, 71.27.+a, 71.28.+d

I. INTRODUCTION

The cobaltates Na_xCoO_2 are layered oxide materials somewhat similar to the cuprates in as much as the charge doping of the CoO_2 layers is controlled on a large range by variation of the Na content. This can be put in parallel with the doping of the cuprates by chemical substitutions on the layers separating the CuO_2 planes. One significant difference with the cuprates is that the Co ions of the CoO_2 plane are ordered on a triangular lattice and not on a square lattice as for the CuO_2 plane of the cuprates. In this configuration, the large crystal field on the Co site favors a low spin state in which orbital degeneracy influences significantly the electronic properties and may yield large thermoelectric effects.[1] A rich variety of other physical properties ranging from ordered magnetic states,[2] high Curie-Weiss magnetism and metal-insulator transition,[3] superconductivity,[4] etc., have then been observed on the cobaltates.

In most cases, the theoretical calculations considered to explain the physical properties of cuprates and cobaltates have assumed uniform delocalization of the carriers in the layers[5] and the incidence of the Coulomb potential of the ionic dopants has been generally considered as unimportant.

Experimentally though, the disorder due to the dopants has been shown to have an important incidence on the local electronic properties in the cuprates: it can blur the physical properties and may drive as well system specific, that is, nongeneric properties of the CuO_2 planes. For instance, static stripe charge organization of the CuO_2 planes have been seen only on specific systems such as $La_{2-x}Ba_xCuO_4$ for which static distortions lead to an orthorombicity of the structure.[6] Some anisotropic electronic properties of $YBa_2Cu_3O_{6+x}$ compounds might as well tentatively be associated with the incidence of the ordered CuO chains, which drive the doping of the CuO_2 planes.[7]

In the cobaltates, NMR experiments and structural investigations have given evidence that for $x \geqslant 0.5$, a large interplay occurs between atomic arrangements and electronic properties, as the Na atoms are found to be ordered.[8–13] It has been shown earlier that this ordering is associated quite systematically with cobalt charge disproportionation into 3^+ and $\approx 3.5^+$ Co charge states.[10,14–16] As the cobalt ions in sodium cobaltates are in low-spin configurations, the Co^{3+} has an electronic spin $S = 0$ and appears to be inert magnetically, when compared to the other Co sites with higher-charge state on which holes delocalize (formally Co^{4+} should have $S = 1/2$). However, the actual Na atomic order, the organization of the Co sites, and their electronic properties have not been so far determined experimentally, except for the case of $x = 1/2$ where such a large charge differentiation does not occur.[17,18] This did not therefore permit yet any theoretical calculations, even in the local density approximation (LDA), based on an actual structure.

We have, however, established for long that one specific structure of Na_xCoO_2 was quite stable for $x \approx 0.7$ and we could ascertain recently that it corresponds to a $x = 2/3$ atomic structure, which could be determined by combining NMR and NQR experiments.[19] The Na organization in this structure, which agrees with GGA calculations,[20] consists of two Na atoms on top of Co sites (the Na1 sites) and six on top of Co triangles (the Na2 sites). This twelve-Co unit cell and the stacking between planes has been confirmed by x-ray diffraction experiments.[21] It results in a differentiation of four cobalt sites in the structure, two nearly nonmagnetic Co^{3+} and two more magnetic sites constituting a kagome sublattice of the triangular Co lattice on which the holes are delocalized (see Fig. 1).

Let us point out that a conflicting suggestion concerning the structure of this phase has been proposed in Ref. 22. In Appendix A, we demonstrate that our data are quite

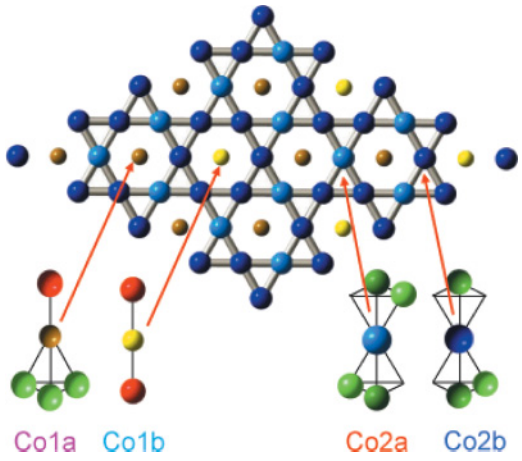

FIG. 1. (Color online) Two-dimensional structure of the Co planes of $Na_{2/3}CoO_2$ compound and the Na environments of the four Co sites differentiated in this structure are displayed. Cobalts in the Co1a and Co1b positions have a threefold symmetry and one or two sodium ions in Na1 position (red balls) as nearest neighbors, which drive them into a nonmagnetic Co^{3+} charge state. In the Co2a and Co2b positions, cobalts have nearest neighbors sodium ions in Na2 positions (green balls). The small difference of local environment of these two Co sites only yields negligible distinction between their electronic properties. This results in a two-dimensional structure where these Co sites form a kagome lattice.[19,21]

incompatible with this alternative structure, and that nothing allows so far to establish the occurrence of oxygen vacancies in our samples.

In the present paper, we shall present a further important experimental step, which consists in the determination of a full set of ^{59}Co NMR data that, together with NQR data, allow us to unravel the electronic properties of the four considered Co sites. We confirm that the electronic structure resumes in two types of Co sites, the nonmagnetic Co1 sites with charge state 3^+ and the Co2 sites on which holes delocalize. The magnetic properties sensed by all four sites have a single T-dependent behavior, which confirms a single band picture suggested initially.[14] We evidence unexpected large anisotropies of the magnetic NMR shift and spin lattice relaxation of the Co2 sites, which have direct implications on the electronic structure of the CoO_2 plane. These results should trigger realistic calculations to explain the correlated electronic structure of these compounds and their evolution with hole doping.

The paper is organized as follows. Sections II–V contain all experimental aspects of the paper, while in Sec. VI, we collected and discussed all the results, which are relevant for further theoretical considerations.

In Sec. II, we recall briefly the methods used to synthesize single-phase samples for $x = 2/3$ and to orient the samples in an applied field. More details on the NMR tests of the quality of the sample alignment are given in Appendix B. In Sec. III, we recall some basics of the NMR spectroscopy of nuclear spins $I > 1/2$ in presence of electric-field gradients (EFG), which induce quadrupole effects. We report then the ^{59}Co NMR spectra detected in Na_xCoO_2 samples when the field is applied in both directions, $H \parallel c$ and $H \perp c$, and the experimental procedures used to separate the contributions of the different sites to the NMR spectrum. We describe then the simulations of the NMR spectra that allowed us to evidence the large in-plane anisotropy of the NMR shift of the magnetic sites.

In Sec. IV, we present the T dependencies of the NMR shifts of all Co sites in the structure and compare them to that observed on the Na NMR (technical details are reported in Appendix C). This allowed us to separate the T-dependent spin contribution to the NMR shifts from a T-independent term that we assign to an orbital contribution. We evidence that both terms are nonaxial on the Co2 sites.

In Sec. V, the technical aspects of the measurements of the ^{59}Co NMR spin lattice relaxation are presented and the data obtained on the two types of cobalt sites are analyzed by comparing the Co T_1 data to that taken formerly on ^{23}Na. This permits us as well to separate the spin and orbital contributions to $(T_1T)^{-1}$. The anisotropies of the data for the spin contributions can be explained by those obtained for the hyperfine coupling. These results allow us as well to demonstrate that the spin and orbital contributions to $(T_1T)^{-1}$ are at least an order of magnitude larger for Co2 than for Co1 sites.

In Sec. VI, we then discuss the ensemble of results on the EFG, the NMR shifts, and $(T_1T)^{-1}$ data. While so far, the qualitative aspects of the data led us to consider that the Co1 sites were Co^{3+}, the measured parameters allow us to get a little bit further and to obtain an upper limit on the charge occupancy of the Co1 sites. More importantly, this allows us to consider the origin of the anisotropy on the Co2 sites and to conclude that it results from the distribution of holes between the axial a_{1g} orbitals and the in-plane e'_g orbitals on the Co2 site.

II. SAMPLE PREPARATION AND EXPERIMENTAL TECHNIQUES

Experiments on sodium cobaltates Na_xCoO_2 have been performed on both powders and single crystals. Usually, NMR experiments, which provide information on the bulk of the samples are expected to bring more information on single crystals than in powder samples. However, this has not be proven to be the case so far.[16,23] Indeed, we have shown that homogeneous single-phase powder samples can be synthesized and can be well controlled by x rays and NMR.[10] Also, the penetration of rf magnetic field into conducting cobaltates single crystals is limited by the skin effect. Thus, for our study, we used powder samples. However, as they consist of particles oriented randomly, the resulting angular distribution of quadrupole splittings introduces, as well, some difficulties in the analysis of the NMR spectra.

A. Samples preparation

The methods that have been used to synthesize reproducibly single-phase powder samples with sodium content $x = 0.67$ have been reported in Ref. 21. As described there, we used three different routes to synthesize homogeneous single-phase samples of $Na_{2/3}CoO_2$ compounds: (1) direct synthesis from a stoichiometric composition of Co_3O_4 and Na_2CO_3, (2) from a mixture of cobaltates with calibrated compositions synthesized previously (such as $Na_{1/2}CoO_2$ and $Na_{0.71}CoO_2$)[10] taken in a

proper ratio, and (3) by deintercalation of Na from $Na_{0.71}CoO_2$ by annealing it at 700 °C (out of its own stability temperature range).

Whatever the synthesis procedure used, the x-ray spectra of these $Na_{2/3}$ CoO_2 samples displayed the same c axis parameter and diffraction spectra, including the satellite Bragg peaks due to Na order.[21] However, we noticed an important difference between these materials regarding the possibility to orient them in a magnetic field.

B. Powder-sample alignment

As the room-temperature susceptibility of sodium cobaltates is known to be anisotropic,[24] we have used this anisotropy to align the single crystallites of powder samples in a 7-T field by mixing the samples with Stycast 1266 epoxy resin, which cured in the field. Thus, in our samples, crystallites c axes were aligned in the same direction, but ab planes of different crystallites were randomly distributed.[25] To be successful, this procedure requires a powder in which individual grains should be single crystallites and should not form clusters. Also, the shape and packing of the grains should not prevent them rotating freely in the magnetic field.

The best aligned samples were obtained from powders that were directly synthesized along route (1) with grain sizes of 50–100 micrometers, but a residual unreacted Co_3O_4 could not be avoided in many cases and the corresponding ^{59}Co NMR signal of Co_3O_4 could be seen in the spectra. The powders obtained along route (3) also usually align well in the magnetic field. Those synthesized along route (2) were most difficult and sometimes impossible to align. In such a synthesis, the small grains are probably randomly welded to each other, so that the final powder does not consist of single crystallites.

For a perfect alignment, the samples should look like a single crystal in the c direction but with full ab plane disorder. Details on the NMR tests of the quality of the sample alignment are given in Appendix B.

Here, we should mention that the Stycast perfectly protects the powder from environment (water) influence.[26] For this Na concentration, the samples prepared six years ago did not show any changes in the NMR spectra.

III. ^{59}Co NMR SPECTRA IN THE $Na_{2/3}CoO_2$

A. NMR background

Generally, in solid state NMR, an atomic nucleus with spin $\vec{I}$ and quadrupole moment Q has its spin energy levels determined by the Zeeman interaction with an external magnetic field $\vec{H}_0$ and the quadrupolar interaction with the electric field gradient (EFG) on the nucleus site. Therefore the Hamiltonian consists of two parts: Zeeman Hamiltonian $\mathcal{H}_Z$ and quadrupolar Hamiltonian $\mathcal{H}_Q$, and can be written as[27,28]

$$\mathcal{H} = \mathcal{H}_Z + \mathcal{H}_Q = -\gamma\hbar\vec{I}(1+\hat{K})\vec{H}_0 + \frac{eQ}{2I(I-1)}\vec{I}\hat{V}\vec{I}, \quad (1)$$

where γ is gyromagnetic ratio.

The physical properties of the studied compound are hidden in the two tensors in this Hamiltonian: magnetic shift tensor $\hat{K}$ and the EFG tensor $\hat{V}$. The principal axes of both tensors are associated with the local structure and assuming that the principal axes (X,Y,Z) of both tensors coincide, the Zeeman and quadrupolar Hamiltonians can be rewritten as

$$\begin{aligned}\mathcal{H}_Z &= -\gamma\hbar\sum_\alpha I_\alpha(1+K_{\alpha\alpha})H_{0\alpha},\\ \mathcal{H}_Q &= \frac{eQ}{2I(I-1)}\sum_\alpha V_{\alpha\alpha}I_\alpha^2\\ &= \frac{h\nu_Z}{6}\left[3I_Z^2 - I(I-1)\right] + (\nu_X-\nu_Y)\left(I_X^2 - I_Y^2\right),\end{aligned} \quad (2)$$

where $\alpha = X,Y,Z$ and the three quadrupolar frequencies

$$\nu_\alpha = \frac{3eQV_{\alpha\alpha}}{[2I(2I-1)h]}$$

are linked by Laplace equation $\sum_\alpha V_{\alpha\alpha} = \sum_\alpha \nu_\alpha = 0$. Therefore it is more common to use two parameters: the quadrupolar frequency $\nu_Q = \nu_Z$, corresponding to the largest principal axis component V_{ZZ} of the EFG tensor, and the asymmetry parameter $\eta = (V_{XX} - V_{YY})/V_{ZZ}$ (here, the principal axes of the EFG tensor are chosen following $|V_{ZZ}| \geqslant |V_{YY}| \geqslant \|V_{XX}|$).

The nuclear spin of ^{59}Co is $I = 7/2$ and therefore, for a given direction of applied magnetic field H_0 relative to the crystallite, the NMR spectrum for a single Co site consists of seven lines: a central line, which corresponds to the $-\frac{1}{2} \leftrightarrow \frac{1}{2}$ transition, and six satellites corresponding to the other $m \leftrightarrow (m-1)$ transitions. The position of the central line is determined by the applied field, the values of the magnetic shift K, and the second-order quadrupolar perturbation.[27] The distance between the two satellite lines $m \leftrightarrow (m-1)$ and $-m \leftrightarrow -(m-1)$ depends on the orientation of the external field with respect to the principal axis of EFG tensor described by the spherical angular coordinates θ and φ and can be expressed as[27]

$$\Delta\nu = \nu_Q\left(m-\tfrac{1}{2}\right)(3\cos^2\theta - 1 + \eta\sin^2\theta\cos 2\varphi). \quad (3)$$

B. Experimental techniques

The NMR measurements were done using a home-built coherent pulsed NMR spectrometer. NMR spectra were taken "point by point"with a $\pi/2 - \tau - \pi/2$ radio-frequency (rf) pulse sequence by varying the magnetic field in equal steps. The minimum practical τ value used in our experiments was 7 μs. The usual $\pi/2$ pulse length was 2 μs.

Experimentally, the value of the magnetic shift (in %) for a given point in the spectrum either in frequency domain or in the field domain can be calculated using

$$K = \frac{\nu - \nu_{\text{ref}}}{\nu_{\text{ref}}} = \frac{B_{\text{ref}} - B}{B}, \quad (4)$$

where ν_{ref} and B_{ref} are reference frequency and field values, respectively, which are connected by the relation $\nu_{\text{ref}} = (\gamma/2\pi)B_{\text{ref}}$. In this work, ^{23}Na shifts are given with respect to the ^{23}Na resonance in a NaCl water solution. The reference for ^{59}Co shift is given for the $\gamma/2\pi = 10.054$ MHz/T value.

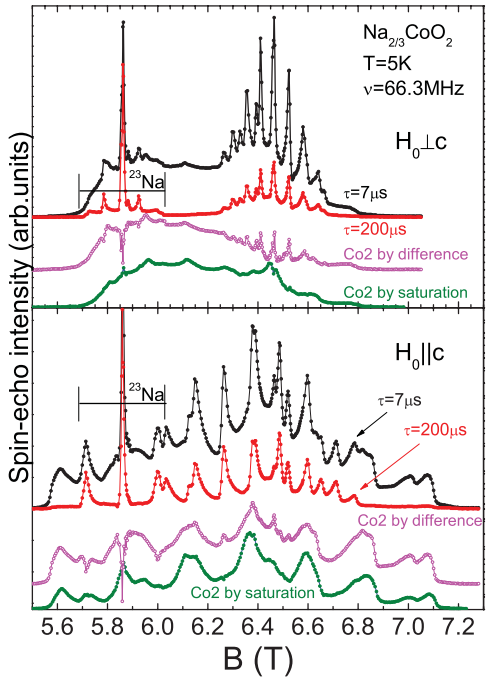

FIG. 2. (Color online) Examples of ^{59}Co NMR spectra of an oriented sample of the $Na_{2/3}CoO_2$ compound taken with the applied magnetic $H_0 \perp c$ (upper panel) and $H_0 \parallel c$ (lower panel). In each panel, the top spectra are taken using a short time interval $\tau = 7\ \mu$s between rf pulses. They involve the NMR signals of all cobalts in the sample. The signals of the slow-relaxing Co1 sites and ^{23} Na are isolated in the second spectra taken with $\tau = 200\ \mu$s. The NMR spectra of the fast-relaxing Co2 sites could be obtained either by subtraction of short-τ and long-τ spectra (Co2 by difference) or by saturation of the slow relaxing Co1 and ^{23}Na NMR signals by an additional rf pulse (Co2 by saturation). Although some remnants of the Na and Co1 signals remain in the difference spectra, the actual quadrupole splitting of the Co2 spectrum is quite well resolved for $H_0 \parallel c$.

C. Decomposition of the spectra in slow- and fast-relaxing components

The raw ^{59}Co NMR spectra in the $Na_{2/3}CoO_2$ compound are complicated; as an example, we show in Fig. 2 the NMR spectra measured in a well-oriented sample at $T = 5$ K for two directions of the applied magnetic field H_0. Former ^{59}Co NMR data[14] taken on this phase have already allowed us to evidence distinct Co NMR lines, but those NMR spectra were somewhat difficult to analyze fully, as one needs to determine altogether the EFG parameters and NMR shifts of the various sites. The experiments were furthermore complicated by the need of a quasiperfect alignment of the powder sample with respect to the applied magnetic field.

We found[14,21] that some Co sites have both very short nuclear spin-spin (T_2) and spin-lattice (T_1) relaxation times; we denote them as Co2 type. The Co sites that have much longer relaxation times could be also isolated; we call these cobalts as Co1 type.

In Fig. 2, we show a decomposition of the experimental spectra in the Co1 and Co2 contributions. The spectrum measured with $\tau = 7\ \mu$s between rf pulses contains contributions of the NMR signals of both type (Co1 + Co2) of ^{59}Co nuclei in the sample, whereas for $\tau = 200\ \mu$s, the only remaining contribution to the signal is that from the slow-relaxing ^{59}Co1 nuclei. One can then obtain the spectrum of the fast-relaxing part Co2 by subtracting the rescaled slow-relaxing part of the spectra from the short-τ spectra. The rescaling can be done empirically by trial and error, or using an estimation of the T_2 decay for the slow-relaxing spectrum. In Fig. 2, the spectrum obtained so for the fast-relaxing part Co2 is shown as "Co2 by difference."

Slow- and fast-relaxing cobalts can be separated as well by the large difference in their spin-lattice relaxation times.[21] It is possible to suppress (or more correctly, to saturate) the signals of ^{23}Na and slow-relaxing Co1-type sites by using an additional $\pi/2$ pulse with some delay (usually 400–1000 μs) before the $\pi/2 - \tau - \pi/2$ pulse sequence. In the spectrum obtained after such a pulse sequence, the intensities of the slow-relaxing cobalt lines are reduced and the lines of the fast-relaxing cobalts are better resolved. Spectra of Co2 obtained by this method are shown in Fig. 2 as "Co2 by saturation."

The shapes of the fast-relaxing Co2 NMR spectra obtained by the two methods are not exactly the same as one can see in Fig. 2. The compliance between the two methods is much better when the external magnetic field is applied parallel to the c axis of the sample. The main reason for the discrepancy is that the nuclear relaxation rates differ in the different parts of the NMR spectra. Therefore it is not so easy to subtract fully or to suppress fully the Co1 spectra, so that some remanent of the intense Co1 lines remains in the "Co2 by difference" spectra. Also, the overlap with the ^{23}Na NMR signal creates additional difficulties; one can see the residual traces of the sodium signal in the obtained Co2 spectra.

D. Slow-relaxing Co1 NMR spectra

Figures 3 and 4 show spectra of the slow-relaxing Co1 at temperatures 5 and 60 K, respectively. These experimental spectra are quite simple as in both directions of applied magnetic field, $H_0 \perp c$ and $H_0 \parallel c$, they are nearly symmetric with respect to the center of the spectra. The largest splitting between satellites for slow-relaxing Co1 is observed when the applied magnetic field H_0 is parallel to the c axis of the sample. This fact demonstrates that the main principal axis Z of the EFG tensor for Co1 in the $Na_{2/3}CoO_2$ compound is parallel to the crystallographic c axis. The fact that the distance between outer singularities in both directions $H_0 \perp c$ and $H_0 \parallel c$ scales as $1 : 2$ shows that these cobalt sites have an axial EFG tensor with asymmetry parameter η close to zero [see Eq. (3)].

The ^{59}Co NMR spectra of the slow-relaxing Co1 can be described by only two unequivalent cobalt sites, which we assign to the Co1a and Co1b sites of Fig. 1. In Figs. 3 and 4, we show computer simulations of the ^{59}Co NMR spectra that we could perform. As one can see, the agreement between the simulated spectra and the data is very good. These simulations of the NMR spectra allow us to deduce ν_Q, η, and the magnetic shift $K_{\alpha\alpha}$ of the central line for the two Co1 sites, which are summarized in Table I.

These results are in good agreement with the parameters deduced from ^{59}Co NQR spectra, which also display two slow-relaxing sites.[21] Moreover, the simulation of the ^{59}Co NMR spectra also confirm the ratio $2 : 1$ between the line intensities

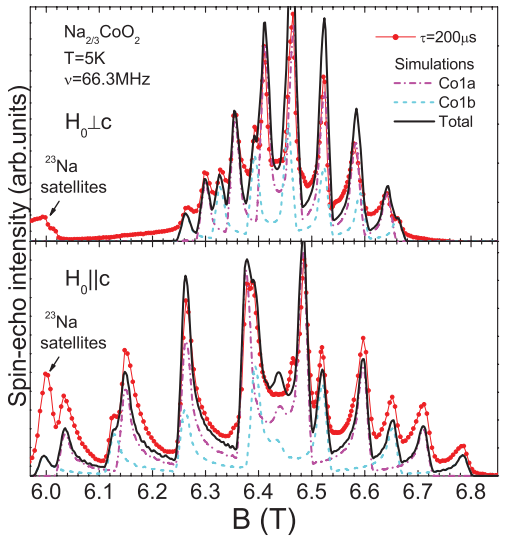

FIG. 3. (Color online) ^{59}Co NMR spectra [(red) dots joined by a full line] of the slow-relaxing Co1 sites measured at $T = 5$ K in the two directions of the applied magnetic field H_0, which were shown in Fig. 2. The simulation of the spectra of Co1a site are shown by (magenta) dash-dotted lines, those of the Co1b spectra are shown by (cyan) dashed lines. The solid black line corresponds to the sum of the Co1a and Co1b simulated spectra.

corresponding to the Co1a and Co1b sites as can be seen in Figs. 3 and 4.

E. Details of the simulations of the NMR spectra

The simulation procedure used to reproduce the powder NMR spectra requires an averaging of computed signals for all

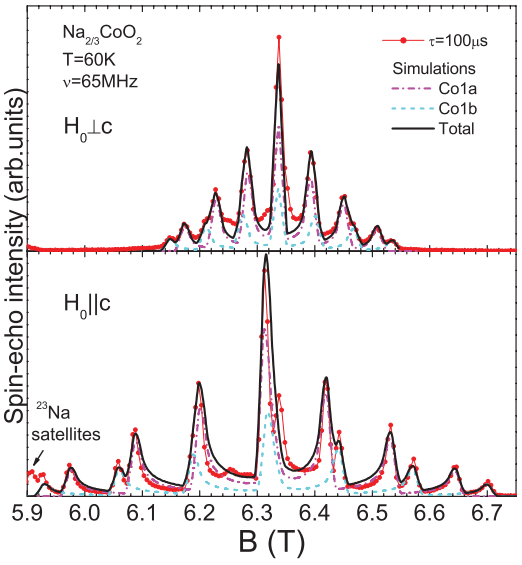

FIG. 4. (Color online) Experimental ^{59}Co NMR spectra [(red) dots joined by a full line] of the slow-relaxing Co1 sites measured at $T = 60$ K in the two directions of the applied magnetic field H_0. The simulation of the spectra of Co1a site are shown by (magenta) dash-dotted lines, those of the Co1b spectra also shown by (cyan) dashed lines. The solid black line corresponds to the sum of the Co1a and Co1b simulated spectra.

TABLE I. Parameters used in Hamiltonian (2) for computer simulations of the ^{59}Co NMR spectra shown in Figs. 3–6 for different cobalt sites in $Na_{2/3}CoO_2$. The principal components of the tensors are given in the principal axes (X,Y,Z) of the EFG tensor. Site occupancy ratios Co1a/Co1b/Co2a/Co2b = 1/2/3/6 were used in the simulations.[19]

		Co1a	Co1b	Co2a	Co2b
	K_{XX}	1.93	2.08	9.52	10.4
	K_{YY}	1.93	2.08	4.36	4.76
NMR	K_{ZZ}	3.48	3.20	3.54	3.80
	ν_Q[a]	1.19	1.386	2.276	2.591
5 K	η	0	0	0.362	0.358
	ν_X[a]	−0.595	−0.693	−0.73	−0.83
	ν_Y[a]	−0.595	−0.693	−1.55	−1.76
	K_{XX}	1.98	1.98	5.19	6.0
NMR	K_{YY}	1.98	1.98	2.80	3.31
	K_{ZZ}	2.67	2.72	2.67	3.72
60 K	ν_Q[a]	1.165	1.340	2.19	2.55
	η	0	0	0.362	0.358
NQR	ν_Q[21]	1.193(1)	1.392(1)	2.187(1)	2.541(1)
4.2 K	η[21]	$\leqslant 0.017$	$\leqslant 0.016$	0.362(5)	0.358(4)

[a] Since in the NMR the sign of the EFG cannot be determined, the sign of values of ν_α could be reversed.

possible orientations of the powder particles. In our samples, the c axes of the crystallites are aligned but the a or b axes are at random. To simulate a possible imperfect alignment of the powder particles, we introduced in our simulation a distribution of crystallite c axes orientations, which we described by a Lorentzian function. For well-oriented samples (like in Fig. 2), the deviation of c axis orientations was within $\pm 5^\circ$. Such an angular distribution described very well the ^{23}Na NMR spectra (see Appendix B) and has been used then in the simulations taken for all cobalt sites in a given sample (see Figs. 3–6).

Simulations of the spectra were done taking into account not only the splittings of the energy levels described by the Hamiltonian of Eq. (2) but also the transition probabilities due to the radio frequency field excitation using the algorithm described in Ref. 29. Also to simulate the broadening of the NMR lines, we used a triangular filtering function with bandwidth 0.15 MHz for both Co1 and Co2 sites at $T = 60$ K. At $T = 5$ K, the larger broadening of the Co2 site spectrum required an increase of this bandwidth to 0.5 MHz, while 0.15 MHz could be kept for the Co1 sites.

F. Fast-relaxing Co2 NMR spectra

Figures 5 and 6 show the spectra of the fast-relaxing Co2 at temperatures 5 and 60 K, respectively. Despite the difficulties in obtaining fast-relaxing Co2 NMR spectra, some facts can be settled. First of all, the largest splitting between satellites for Co2 is observed for $H_0 \parallel c$. Therefore, for Co2, the main principal axis Z of the EFG tensor is parallel to the crystallographic c axis in the $Na_{2/3}CoO_2$ compound.

The Co2 spectrum for $H_0 \parallel c$ at $T = 60$ K (see Fig. 6) is quite simple, well resolved, and clearly evidences two inequivalent Co2 sites with different values of quadrupole

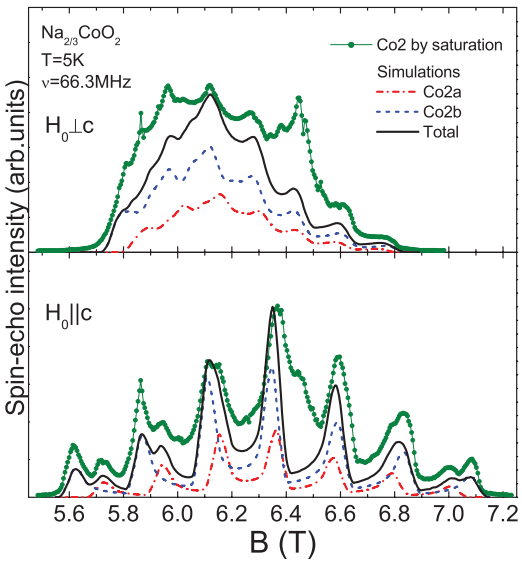

FIG. 5. (Color online) ^{59}Co NMR spectra [(green) dots joined by a full line] of the fast-relaxing Co2 sites measured at $T = 5$ K in the two directions of the applied magnetic field H_0. Those were obtained by saturation of slow-relaxing Co1 and ^{23}Na NMR signals and are taken from Fig. 2. The simulation of the spectra of the Co2a site are shown by (red) dash-dotted lines, those of the Co2b spectra also shown by (blue) dashed lines. The solid black line corresponds to the sum of the Co2a and Co2b simulated spectra. The large deviations seen for $B \approx 6.45$ and $\approx$5.9 T are due to the imperfect saturation of the Co1 and Na contributions.

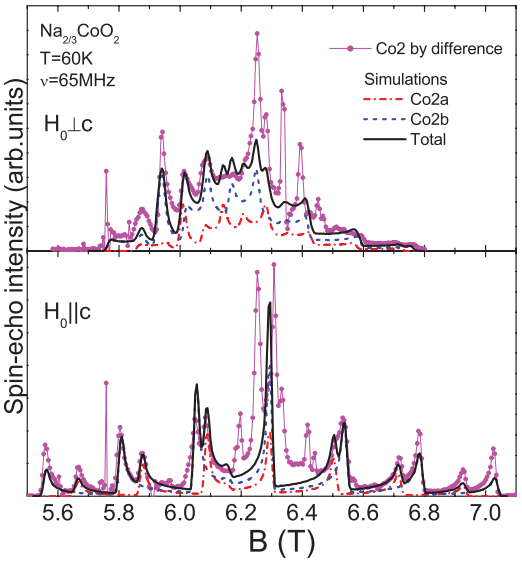

FIG. 6. (Color online) ^{59}Co NMR spectra [(magenta) dots joined by a full line] of the fast-relaxing Co2 sites measured at $T = 60$ K in the two directions of the applied magnetic field H_0. Those were obtained by subtraction of long-τ spectra from the short-τ spectra. The simulation of the spectra of the Co2a site are shown by (red) dash-dotted lines, those of the Co2b spectra also shown by (blue) dashed lines. The solid black line corresponds to the sum of the Co2a and Co2b simulated spectra. The large peaks between 6.2 and 6.4 T are remnants of the Co1 NMR signals, incompletely subtracted.

frequency ν_Q; we denote these sites as Co2a and Co2b. The relative intensities of the NMR signals of these sites corresponds to a ratio Co2a : Co2b close to 1 : 2. These facts are in very good agreement with the ^{59}Co NQR spectra, which also display two fast-relaxing sites with a similar intensity ratio.[21]

At low temperature $T = 5$ K, the Co2 spectrum in the $H_0 \parallel c$ case (see Fig. 5) is less resolved due to the large magnetic broadening of the lines, but the satellites of the two sites could still be seen.

If we compare now the Co1 and Co2 NMR spectra measured in the $H_0 \perp c$, it is easy to see that Co2 spectra are asymmetric with a larger intensity in the lower fields. At $T = 60$ K, some lines are resolved with clear singularities, but at $T = 5$ K, it becomes nearly impossible to resolve the different lines and we could only detect very weak singularities. As the orientation procedure of our samples is such that the ab planes of different crystallites are randomly distributed, then the experimental spectra in the $H_0 \perp c$ direction are powder spectra. This explains why they are less resolved than the $H_0 \parallel c$ spectra. However, some singularities could still be perceived even in the broadened spectrum at $T = 5$ K (see Fig. 5). Such a complexity is apparent as well in the data taken by many other groups in sodium cobaltates with sodium content $x \approx 0.7$.[30,31] Comparing our oriented powder NMR spectra with NMR data taken on single crystals[16,23] allows us to conclude that twinning of the ab plane is quite common in those single crystals.

Therefore the analysis of a single $H_0 \perp c$ spectrum of Co2 appears quite difficult. Independently of the method used to isolate the fast relaxing Co2 spectra, we do, however, find that the positions of the different singularities in the Co2 spectra are the same as one can see in Fig. 2. As usual, such singularities in a powder NMR spectrum appear at positions where the two principal axes X and Y of the EFG and magnetic shift tensor in the ab plane correspond to extremal positions of the NMR signal for randomly distributed crystallites. Furthermore, as was shown in Ref. 14, the sodium and cobalt sites in the $Na_{2/3}CoO_2$ compound feel a common T dependence of the spin susceptibility, which we could determine directly by measuring the ^{23}Na magnetic shift $^{23}K(T)$.[9] We did then study the evolution of the positions of the singularities in the Co2 spectrum versus temperature. By plotting these singularities versus the spin susceptibility as monitored by ^{23}K, the temperature being then an implicit parameter, we could sort out those singularities that correspond to Co2 central lines and those that can be assigned to quadrupolar satellites, as detailed in Appendix C.

This allowed us to resolve then fully the EFG and shift tensors of Co2a and Co2b sites and to understand that not only the EFG tensor but also the shift tensors are highly asymmetric. We could then succeed to perform a full simulation of the ^{59}Co NMR spectra of the fast-relaxing cobalts in the two field directions, as shown in Figs. 5 and 6, with the parameters collected in Table I. There, we also reported the parameters measured for the Co1a and Co1b sites, as obtained from the simulations done in Figs. 3 and 4. As one can see, the obtained values of the quadrupole frequency ν_Q and of the asymmetry parameter η for all sites are in good agreement with the values obtained by NQR.[21]

IV. T DEPENDENCE OF THE COBALT MAGNETIC SHIFTS

The principal components of the magnetic shift tensor for the cobalt site i in a direction α consist on three parts

$$K_{i,\alpha} = K_{i,\alpha}^{\rm dia} + K_{i,\alpha}^{\rm orb} + K_{i,\alpha}^{\rm spin} = K_{i,\alpha}^{\rm dia} + A_{i,\alpha}^{\rm orb}\chi_{i,\alpha}^{\rm orb} + A_{i,\alpha}^{s}\chi_{i,\alpha}^{s}(T). \quad (5)$$

Here, $K_{i,\alpha}^{\rm dia}$ is the chemical shift due to the diamagnetic susceptibility of the inner shell electrons, $K_{i,\alpha}^{\rm orb}$ reflects the on-site orbital effect of the valence electrons, proportional to the orbital part of the electronic susceptibility $\chi_{i,\alpha}^{\rm orb}$, which is usually temperature independent. The last term, the spin shift $K_{i,\alpha}^{\rm spin}$, is proportional to the local electronic spin susceptibility $\chi_{i,\alpha}^{s}(T)$.

The remarkable feature of the $Na_{2/3}CoO_2$ phase of the sodium cobaltates is the large low-T variation of this last term, which, as already pointed out above, allowed us to resolve the Co NMR spectra.[10] The ^{23}Na NMR has negligible chemical and orbital NMR shifts and is largely dominated by the T-dependent spin term, which has been found nearly isotropic.[9] So the comparison of $^{59}K_{i,\alpha}$ with the isotropic contribution $^{23}K_{\rm iso}$ also allowed us to separate the orbital and spin contributions to the cobalt magnetic shift, as detailed below.

A. Co1 shifts

In Fig. 7(a), we show the T dependence of the magnetic shifts of Co1a and Co1b sites, which are plotted in Fig. 7(b) versus the NMR shift of ^{23}Na. For Co1a and Co1b sites, the Z components of the magnetic shift are quite similar, with a substantial T dependence, which is proportional to ^{23}K at temperatures below 150 K.

The in-plane X and Y components of the shift are indistinguishable for Co1a and Co1b sites, and their shift value does not change from 150 down to 40 K. Below this temperature, some small difference in the in-plane shifts for Co1a and Co1b sites appears. This was also seen by others,[31] which points out that this effect is somewhat characteristic of this $x = 2/3$ phase of Na cobaltates. But as one can see in Fig. 7, these distinct variations of NMR shifts of Co1a and Co1b are quite small when compared with the T variations of the NMR shifts of both Co1 sites for $H_0 \parallel c$. So we can consider so far that the in plane shift of the Co1 sites is practically T independent below 150 K.

Using Fig. 7(b), one can get the slopes of the linear fits of ^{59}K versus ^{23}K, which give the relative magnitudes of the spin contributions $K_{i,\alpha}^{\rm s}/{}^{23}K$, while the $^{23}K = 0$ intercepts give the estimates of the T-independent contribution to the ^{59}Co NMR shift. The values found here, reported in Table II, are much larger than those expected for the chemical shift $K_{i,\alpha}^{\rm dia} \lesssim 0.1\%$. They are obviously dominated here by the Co orbital NMR shift $K_{i,\alpha}^{\rm orb}$, so that we have neglected $K_{i,\alpha}^{\rm dia}$ in all our analyses.

But, as seen in Fig. 7, significant increases of $^{59}K_1^{\alpha}$ with respect to the low-T linear ^{23}K dependence are observed for $T \gtrsim 150$ K, that is for $^{23}K < 0.08$. Those increases are associated with the onset of Na motion, which has been detected at ≈200 K from ^{23}Na data in Ref. 10. There, we have discussed that this Na motion induces a significant Co1-Co2 site exchange, which induces such an increase of Co1 NMR shifts, while the charge disproportionation already occurs above room temperature.

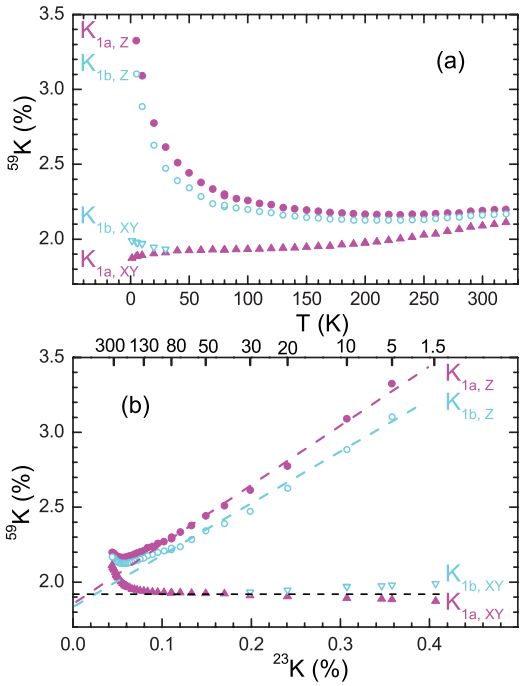

FIG. 7. (Color online) (a) T dependencies of the ^{59}Co NMR shifts of the Co1a [filled (magenta) symbols] and Co1b [open (cyan) symbols] sites for two directions of the external magnetic field H_0. For $H_0 \parallel Z$ (circles), the Co1a and Co1b shifts exhibit the same T dependence with a small difference in absolute values. In the $H_0 \perp Z$ direction, for both sites Co1a and Co1b, the T dependence is much weaker and a small difference between the shifts of these sites appears only below $T = 40$ K. For both Co1a and Co1b sites, the magnetic shifts are axial. (b) The data of (a) are plotted versus the ^{23}Na NMR shift showing linear slopes at low temperatures and deviations from this linear dependence above 100 K. Such low-T linearity allowed us to determine the orbital $K_{ii}^{\rm orb}$ and spin $K_{ii}^{\rm s}$ contributions to ^{59}K for all three directions $i = X,Y,Z$ (see Table II).

B. Co2 shifts

In Fig. 8(a), we show the T dependencies of the magnetic shifts of Co2a and Co2b sites and in Fig. 8(b), they are shown versus ^{23}K. In this figure, we put some experimental points, which were determined accurately at specific temperatures,

TABLE II. ^{59}Co magnetic shift parameters obtained for the four cobalt sites.

Site	Co1a	Co1b	Co2a	Co2b
$K_{XX}^{\rm s}/{}^{23}K$	−0.2(2)	0.2(2)	17.9(4)	19.9(4)
$K_{YY}^{\rm s}/{}^{23}K$	−0.2(2)	0.2(2)	7.1(3)	7.9(3)
$K_{ZZ}^{\rm s}/{}^{23}K$	4.0(2)	3.5(2)	4.6(2)	5.2(2)
$K_{XX}^{\rm orb}(\%)$	1.92(2)	1.92(2)	3.1(2)	3.3(2)
$K_{YY}^{\rm orb}(\%)$	1.92(2)	1.92(2)	2.1(2)	2.3(2)
$K_{ZZ}^{\rm orb}(\%)$	1.86(5)	1.86(5)	1.92(5)	1.95(4)

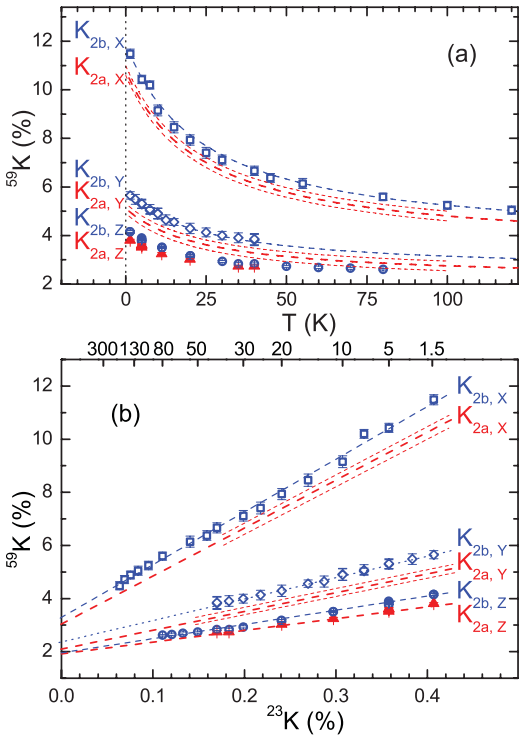

FIG. 8. (Color online) (a) T dependencies of the ^{59}Co NMR shifts of the Co2a [(red) closed symbols and (red) dashed lines] and Co2b [(blue) open symbols and (blue) dashed lines] sites for the three directions of the external magnetic field H_0 parallel to the X,Y,Z principal axes of the EFG tensor. The method used to determine the data for $H_0 \parallel X,Y$ directions is detailed in Appendix C. (b) The data of (a) are plotted versus the ^{23}Na NMR shift. The linear variation of ^{59}K vs ^{23}K allowed us to determine the orbital $K_{ii}^{\rm orb}$ and spin K_{ii}^{s} contributions to the ^{59}K for the three directions $i = X,Y,Z$ (see Table II).

but due to the relatively small number of Co2a sites, the intensity of its NMR signal is weak. For this site, we plot lines corresponding to the K_X and K_Y components of its shift obtained from the analysis detailed in Appendix C.

As one can see in Fig. 8(b), a linear dependence is found for all components of the magnetic shift for both Co2a and Co2b sites below 120 K in a range where no sign of Na motion could be seen. So this figure in combination with Fig. 7(b) confirm that all four cobalt sites pertain, indeed, to a unique sodium cobaltate phase in which a single T variation characterizes the local $\chi_{i,\alpha}^{s}(T)$. We collected in Table II the relative magnitude of the spin contributions $K_{i,\alpha}^{s}/^{23}K$ and $K_{i,\alpha}^{\rm orb}$ for all three components of the magnetic shift for the Co2a and Co2b sites together with those of the Co1 sites.

While the magnetic shift tensors are axial for the Co1a and Co1b sites, we see in Table II that both Co2a and Co2b sites demonstrate strong in-plane anisotropy of both the orbital shift and the spin hyperfine coupling. This totally unexpected anisotropy is a quite important observation achieved in the present investigation. In our previous paper concerning the ^{59}Co NMR in this phase[14] as well as in all the existing publications,[16,23,30,31] such anisotropy was not anticipated. This , consequently, led us to invoke a third group of axial cobalt sites, Co3, with large shift values. In Appendix B, we detail why imperfect alignment of the sample powder led us as well to overlook initially this anisotropy.

V. ^{59}Co SPIN-LATTICE RELAXATION

When thermal equilibrium of the nuclear spins is disturbed by rf pulses, the equilibrium nuclear magnetization is recovered by various relaxation processes that reflect the interactions in the spin system and the magnetic and electronic properties of the materials. The recovery of the nuclear magnetization along the applied field operates through nuclear spin-lattice relaxation (NSLR) processes characterized by the spin-lattice relaxation time T_1 or by the nuclear spin-lattice relaxation rate $1/T_1$.

In systems with unpaired spins, the dominant T_1 process is due to local field fluctuations induced by the dynamics of the local electronic magnetization. Theoretically, the spin contributions to $(T_1T)^{-1}$ may be written using the imaginary part of the Co dynamical electron spin-susceptibility $\chi''(\mathbf{q},\nu_n)$ as

$$(T_1T)^{-1} = \frac{2\gamma_n^2 k_B}{g^2\mu_B^2}\sum_{\mathbf{q}}|A(\mathbf{q})|^2\frac{\chi''(\mathbf{q},\nu_n)}{\nu_n}, \qquad (6)$$

where $A(\mathbf{q}) = A_0 + \sum A_i e^{i\mathbf{q}\mathbf{r}_i}$ is the wave-vector, $\mathbf{q}$, dependent hyperfine form factor, which depends on the hyperfine interaction between the observed Co nuclear and electron spins at the same site A_0 and the hyperfine interaction with electron spins at nearest-neighbor Co sites A_i.[32]

Our measurements of the ^{23}Na NSLR temperature dependence allowed us to establish that in sodium cobaltates with sodium content $x > 0.6$ the dominant correlations in the electron spin system are ferromagnetic, while for lower sodium contents antiferromagnetic correlations take over.[10,15]

Equation (6) applied to different nuclei tells us that NSLR data should be similar for all nuclei in the absence of any cancellation at some specific $\mathbf{q}$ vector due to the form factor associated with the geometrical position of the nuclear site with respect to the magnetic atoms. So the comparison of ^{59}Co and ^{23}Na NSLR could help us to better characterize the dynamic susceptibility. We report then here the results of a detailed study of the ^{59}Co NSLR in this $Na_{2/3}CoO_2$ phase. First, we demonstrate the consistency and validity of our measurements, and then compare the results for the different Co sites. We follow as well the procedure used for the shift measurements and compare directly the Co and Na T_1 data.

A. Experimental techniques

To study the nuclear spin-lattice relaxation process of the ^{59}Co we have used the usual magnetization inversion recovery method with three pulses: $\pi - t - \pi/2 - \tau - \pi$. In this sequence, the first pulse rotates the magnetization by 180° and the longitudinal magnetization recovered after time t is measured with a spin-echo sequence with interval τ. The dependence of the spin-echo intensity on delay time t allows to monitor the recovery of the nuclear magnetization associated with a given NMR transition:

$$M(t) = M_0[1 - BR(t)]. \qquad (7)$$

TABLE III. Parameters λ_i and a_i of the theoretical spin-lattice relaxation function (8) for different transitions of ^{59}Co for the case of magnetic relaxation by weak fluctuating magnetic fields (based on Refs. 33 and 34).

λ_i	28	21	15	10	6	3	1
Transition	a_1	a_2	a_3	a_4	a_5	a_6	a_7
$-\frac{1}{2} \leftrightarrow +\frac{1}{2}$	0.714	0	0.206	0	0.068	0	0.012
$\pm\frac{1}{2} \leftrightarrow \pm\frac{3}{2}$	0.457	0.371	0.001	0.117	0.030	0.012	0.012
$\pm\frac{3}{2} \leftrightarrow \pm\frac{5}{2}$	0.114	0.371	0.366	0.081	0.008	0.048	0.012
$\pm\frac{5}{2} \leftrightarrow \pm\frac{7}{2}$	0.009	0.068	0.206	0.325	0.273	0.107	0.012

Here, M_0 is the thermal equilibrium value of magnetization and the parameter B characterizes the actual magnetization after the first pulse at $t = 0$ (the imperfection of the experimental conditions gave typical values $B \simeq 1.8$ rather than $B = 2$ expected for a perfect π pulse).

The shape of the relaxation function $R(t)$ depends on the nuclear transition sampled. For a two-level nuclear system (like the $I = 3/2$ NQR case), this process is exponential, $R(t) = \exp(-t/T_1)$, and allows a simple experimental determination of T_1.[28] But generally, for $I > 1/2$, the nuclear energy levels are differentiated by the quadrupole interaction with the crystalline electric field [see Eq. (1)]. For very broad NMR spectra as those considered here, the applied first pulse only inverts the populations of some levels, which, for a given frequency, can be selected by properly choosing the applied field. Consequently, the difference in population between adjacent levels that are probed by the rf pulses depends on the populations of the levels that are not hit by the rf pulses. Therefore the magnetization recovery becomes multiexponential,

$$R(t) = \sum_i a_i \exp\left(-\frac{\lambda_i t}{T_1}\right), \tag{8}$$

but is still characterized by a single T_1 value.

The spin-lattice relaxation could be driven either by magnetic or quadrupolar fluctuations that correspond to distinct transition probabilities and λ_i values. However, in the sodium cobaltates, the magnetic relaxation mechanism dominates at least at low T.[21] Using Ref. 33 and 34 we have calculated for our values of η, the a_i and λ_i parameters for the theoretical relaxation functions $R(t)$ for the case of magnetic relaxation by weak fluctuating magnetic fields for the different ^{59}Co transitions (see Table III).

B. ^{59}Co spin-lattice relaxation results

We have already seen by NQR that T_1 data are identical for the Co1a and Co1b sites. They are identical as well for Co2a and Co2b sites but much shorter than on the Co1 sites, which allowed us to confirm that the Co2 sites were indeed the magnetic sites.[21]

Due to the close values of the magnetic shift for all four cobalt sites in the Z direction (see Table II), to avoid cross relaxation between sites, it is of course better to take data on quadrupolar satellite transitions of different sites that are quite separated in frequency (or field). So we have measured the spin-lattice relaxation curves on the outer satellites $+\frac{5}{2} \leftrightarrow +\frac{7}{2}$ for the sites with larger signal intensity, that is, Co1a for the slow-relaxing sites and Co2b for the fast-relaxing sites. In Fig. 9, we display such examples of experimental spin-lattice relaxation curves for Co1a and Co2b sites. One can see there that they can be fitted quite well by the function (8) with the coefficients from Table III. It can also be seen in Fig. 9(a) that the same T_1 value is deduced from the data for the $\frac{3}{2} \leftrightarrow \frac{5}{2}$ and $\frac{5}{2} \leftrightarrow \frac{7}{2}$ transitions for the Co1a nucleus, demonstrating convincingly that the data analysis is reliable and that the relaxation is indeed magnetic.

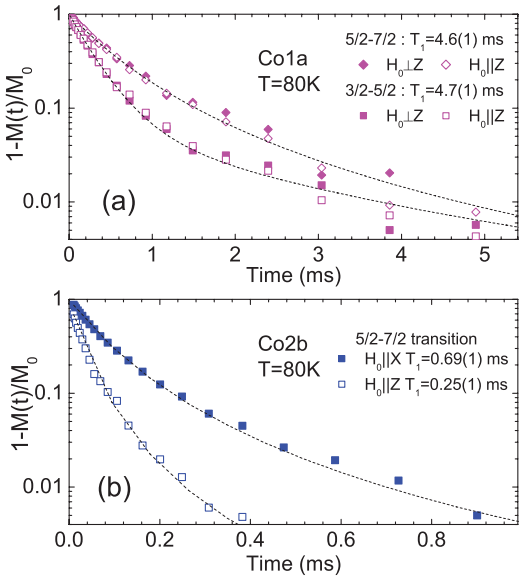

FIG. 9. (Color online) Spin-lattice relaxation curves measured at $T = 80$ K for two orientations of the magnetic field. (a) For Co1a sites, the data shown have been taken on two satellite transitions $\frac{5}{2} \leftrightarrow \frac{7}{2}$ and $\frac{3}{2} \leftrightarrow \frac{5}{2}$. The fits of the data with the magnetization relaxation functions (8), with parameters from the Table III , give a unique T_1 value, independent of the field orientation. (b) For Co2b, similar good fits are obtained for the data, but the relaxation time depends on the field orientation.

We could also evidence in Fig. 9(b) that the T_1 data depend of the orientation of the applied field for Co2, contrary to the isotropic results found for the Co1 sites in Fig. 9(a).

Similarly, in Fig. 10(a), we plotted then the T variation of the Co2b T_1^{-1} data measured in two distinct applied fields, showing that T_1 values measured are identical, which confirms the reliability of the measurements in view of the large spectral changes that occur with increasing field. We also compare there the data taken on Co1a with those on Co2b. The T_1 values differ by a factor as large as 20, which confirms the strong differentiation already found in previous observations done by NQR at low T.[21]

Generally, as given in Eq. (6), the electron spin contribution to the spin-lattice relaxation rate T_1^{-1} is governed by the fluctuations of the transverse components of the effective magnetic field induced at the nucleus by the electronic magnetization. In NMR, the quantization axis is given by the external magnetic field and for the ^{59}Co T_1^{-1}, the dominant term is the fluctuating hyperfine field whose magnitude is proportional to the hyperfine field $|A(\mathbf{q})|$ and local spin

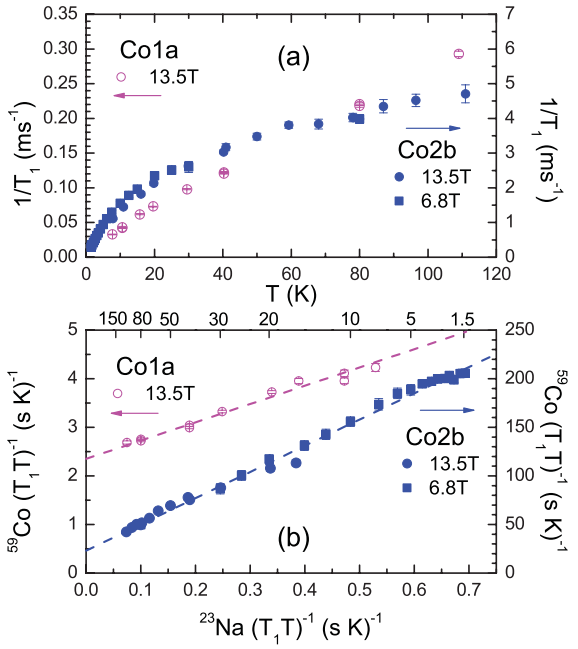

FIG. 10. (Color online) (a) Temperature dependence of the NSLR rate T_1^{-1} measured in $H_0 \parallel c$ orientation for the Co1a (magenta empty circles) and Co2b sites (blue closed circles and squares, taken for two different applied fields). (b) The $(T_1T)^{-1}$ of ^{59}Co of (a) are plotted vs $(T_1T)^{-1}$ values of ^{23}Na, the temperature T being then an implicit parameter in the plot. For both Co1a and Co2b sites the variations are found linear, which allows us to separate the spin and orbital contributions to the ^{59}Co $(T_1T)^{-1}$(see text).

susceptibility $\chi''(\mathbf{q},\nu_n)$. The NMR shift and T_1 data taken on ^{23}Na have given evidence that these electronic susceptibilities are nearly isotropic,[9,10] so the spin contributions to $1/T_1$ on all nuclei are expected to scale with each other and the T_1 anisotropies should be governed by those of the hyperfine couplings $|A(\mathbf{q})|$. For instance,

$$T_{1Z}^{-1} \propto \left(K_{YY}^2 + K_{XX}^2\right) \quad \text{and} \quad T_{1X}^{-1} \propto \left(K_{YY}^2 + K_{ZZ}^2\right).$$

Therefore, as the spin component of the magnetic shift K_{XX} for Co2 is much larger than that for Co1 (see Table II), it is quite natural to find much shorter T_1 values for Co2 than for Co1. Also, as the components of the magnetic shift tensors for Co2 sites are highly anisotropic, with a dominant value for $H_0 \parallel X$, the transverse fluctuating local fields are expected much larger for T_{1Z}^{-1} than for T_{1X}^{-1}, in qualitative agreement with the anisotropy of the T_1 data displayed in Fig. 9(b).

However, for Co1, a distinct situation occurs. As one can see in Fig. 9(a) for Co1a, the spin-lattice relaxation is isotropic, while the spin component to the shift is strongly anisotropic—K_{ZZ} is much larger than the in-plane components, which are vanishingly small—see Fig. 7 and Table II.

To explain that, we considered whether the spin components of the electronic dynamic susceptibility do dominate the relaxation, or is there another independent contribution to $1/T_1$, such as, for instance, an orbital contribution to the spin-lattice relaxation? Indeed, usually for transition metals, two additive contributions to T_1 are expected:

$$\frac{1}{TT_1} = \frac{1}{TT_1^{\text{orb}}} + \frac{1}{TT_1^{\text{spin}}}. \tag{9}$$

So we tried to separate such components similarly to what we had done before for the cobalt shifts (see Sec. IV). Indeed, as was shown in Ref. 10, in the $Na_{2/3}CoO_2$ compound, the ^{23}Na spin-lattice relaxation is largely dominated by the T-dependent spin term, while any orbital contribution is negligible on that nuclear site. So we can plot the values of $(T_1T)^{-1}$ of ^{59}Co versus $(T_1T)^{-1}$ values of ^{23}Na as done in Fig. 10(b). Good linear relations are found for both sites, that is

$$^{59}(T_1T)_Z^{-1} = {}^{23}(T_1T)^{-1} * 3.8(1) + 2.4(1)$$

for Co1a, and

$$^{59}(T_1T)_Z^{-1} = {}^{23}(T_1T)^{-1} * 270(3) + 23(2)$$

for Co2b. This analysis allows indeed to separate in the T_1 data the spin part from an orbital T_1T = constant part.[35] Let us notice that the ratio of the spin contributions for Co2 and Co1 is about $270/3.8 \approx 70$. Such a large ratio compatible with that obtained by NQR[21] is quite expected as the spin part of the Co1 shift in the X and Y directions is practically zero (see Table II).

As for the orbital contribution, one can see in Fig. 10 that it is small with respect to the spin contribution for the Co2 site, while it becomes dominant for the Co1 site. For instance, at $T = 80$ K, the T_1 is totally dominated by the orbital term for the Co1 site, which perfectly justifies the absence of detected T_1 anisotropy on the Co1 site at this temperature. Let us point out, however, that the orbital term is still one order of magnitude larger for Co2 than for Co1.

Overall, these T_1 data are totally compatible with the anisotropy of the Co2 shifts reported in Sec. IV B. We shall discuss further the implication of these results on the electronic properties of this $Na_{2/3}CoO_2$ phase in the following discussion section.

VI. DISCUSSION

We have reached now a rather complete experimental determination of the NMR parameters for the four Co sites formerly detected by NQR,[21] which, together with the ^{23}Na NMR spectra, allowed us to determine the atomic structure of this $Na_{2/3}CoO_2$ phase.[19] The analysis of the NMR shifts and of the magnitude of the EFGs will allow us to confirm here the importance of cobalt charge disproportionation between the nonmagnetic and magnetic sites, that is of the charge order induced in the structure. We shall discuss hereafter how this electronic kagome differentiation is reflected on the orbitals involved at the Fermi level at the different sites of the Co plane. The anisotropy of the EFG and NMR spin shifts will be seen to be related with the hole orbital ordering, which governs the electronic properties of this phase.

A. Site differentiation

The data in Table I allowed us to evidence that for the Co1a and Co1b sites, the symmetry of the magnetic shift tensor $\hat{K}$ is

axial ($K_X = K_Y$), as found before for the EFG tensor ($\eta = 0$ or $\nu_X = \nu_Y$). The local symmetry of these sites had been a key argument used to resolve the crystal structure.[19] We also fully confirm here that the electronic properties are quasi-identical for Co1a and Co1b sites, which are slow relaxing and weakly sensitive to the magnetism.

The knowledge of this actual atomic structure has allowed us also to resolve fully the difficulties connected with the imperfect alignment of the powder grains for some samples, which had initially led us to conclude that the two other Co sites displayed quite distinct nearly axial NMR shifts.[14] The analysis of the extensive set of ^{59}Co NMR spectra done for the two fast relaxing sites Co2a and Co2b allow us to establish that these sites have nearly identical spin shift tensors, which are unexpectedly totally nonaxial, the larger NMR spin shifts being in a privileged X direction in plane. The large anisotropy of the spin contribution to the $1/T_1$ data agrees perfectly with this NMR shift anisotropy, as T_{1Z} is found shorter than T_{1X}.

We therefore established here that these fast-relaxing Co2a and Co2b sites have similar anisotropic orbital and spin shifts and almost identical T_1 values,[19,21] confirming that they contribute identically to the electronic properties and are dominantly responsible for the magnetic properties of this compound.

This allows us then to conclude that although the local environment of Na^+ charges shown in Fig. 1 are quite distinct for the two Co1 sites (or the two Co2 sites), the electronic and magnetic properties only marginally differ within each group of two sites. This establishes that, when dealing with the electronic properties, one might only consider a two-site structure, with Co2 on a kagome planar structure, and Co1 on the complementary triangular structure.

B. Charge ordering

This differentiation of sites had clearly led us to suggest that the ionic characters of the Co1 and Co2 sites are not the same.[19] We have suggested for long that the Co1 sites had an isotropic NMR orbital shift, which is a strong signature that the Co1 sites are themselves nearly Co^{3+}, the orbital shift magnitude being furthermore nearly identical to that found in the band insulator phase Na_1CoO_2,[36,37] in which all Co sites are nonmagnetic Co^{3+}. More accurately, as we are dealing with a metallic system, the filling of the bands involving the Co t_{2g} orbitals at the Fermi level is quite different on the Co1 and Co2 sites, and we can expect that the hole filling ϵ of the t_{2g} orbitals is small on the Co1 site. Let us assume that the hole content on Co2 sites is δ. As the number of holes per CoO_2 formula unit is 1/3, the charge neutrality for the kagome structure implies then $(3\epsilon + 9\delta)/12 = 1/3$, that is

$$\delta = 4/9 - \epsilon/3.$$

1. Isotropic spin susceptibilities and T_1 data

The T-dependent NMR shifts of the Co sites, which scale with that of ^{23}Na, give a measure of the spin susceptibilities on the Co sites. If we consider in Table II the isotropic shifts $K_{\rm iso} = (1/3)\sum K_{\alpha\alpha}$ on the Co sites, we immediately find that the average values for the two Co1 sites $K_{\rm iso}({\rm Co1})/^{23}K \approx 1.3$ is an order of magnitude smaller than that for the Co2 sites $K_{\rm iso}({\rm Co2})/^{23}K \approx 10.6$, which indicates that the unpaired spins are dominantly on the Co2 sites. Similarly, both from NMR and low-T NQR data, we did find a ratio $\approx$70 between the spin contributions to $1/T_1$ for the two sites. Assuming similar hyperfine couplings for the two sites, one could anticipate from these results a ratio of $\sqrt{70} \approx 8$ of the local spin susceptibilities on the two sites, that is $\epsilon/\delta \lesssim 1/8$. This corresponds to an upper limit of 0.06 for epsilon.

2. Isotropic orbital susceptibilities and orbital contribution to $(T_1T)^{-1}$

Let us consider the difference found for the orbital shifts between the Co1 and Co2 sites. While for Co1 sites $K^{\rm orb}$ was found isotropic already in Ref. 14, we do confirm here that $K^{\rm orb}$ is anisotropic in plane for the Co2 sites with a sizable increase of $K^{\rm orb}_{\rm iso}$. We can therefore consider that the contribution of the hole orbitals to the orbital susceptibility is responsible for the deviation of $K^{\rm orb}_{\rm iso}$ with respect to 1.91(3)% found in Na_1CoO_2.[36] In a rough order of magnitude comparison, we might consider then that the hole density on the Co sites is proportional to $K^{\rm orb}_{\rm iso} - K^{\rm orb}_{\rm iso}(x = 1)$, as we already suggested in Ref. 14. We do find then, from the results of Table II, that $K^{\rm orb}_{\rm iso}({\rm Co1}) - K^{\rm orb}_{\rm iso}(x = 1) = -0.01 \pm 0.05(\%)$, while $K^{\rm orb}_{\rm iso}({\rm Co2}) - K^{\rm orb}_{\rm iso}(x = 1) = 0.54(\%)$. This would give again an upper estimate of $\epsilon/\delta \lesssim 1/10$. Similarly, knowing[36] that for Co^{3+} in insulating Na_1CoO_2, the spin-lattice relaxation rate is very weak, one could anticipate that the metallic orbital contributions to $(TT_1)^{-1}$ would be linked to the hole doping on the corresponding site. So there is no surprise to find out that $(TT_1^{\rm orb})^{-1}$ is much larger for Co2 than for Co1.

So the data lead us to consider that we may neglect ϵ as a first approximation and keep $\delta \approx 0.44$, although only accurate band calculations could tell exactly whether the partly filled bands at the Fermi level do not include any partial Co1 hole orbital in the kagome structure.

3. EFG induced by charge order

Let us consider now the quadrupole frequencies ν_Q, which are directly proportional to the EFG on the nuclear site probe. The latter arises from a nonsymmetric distribution of electric charges around it. These charges can originate from nonbonding electrons, electrons in the bonds and charges of neighboring atoms or ions. The components of the EFG tensor can be written as the sum of two terms, the lattice $V^{\rm latt}_{\alpha\alpha}$ and electron $V^{\rm el}_{\alpha\alpha}$ contributions:

$$V_{\alpha\alpha} = (1 - \gamma_\infty)V^{\rm latt}_{\alpha\alpha} + (1 - R_{\rm el})V^{\rm el}_{\alpha\alpha}, \tag{10}$$

where parameters γ_∞ and $R_{\rm el}$ are the Sternheimer antishielding factors, which characterize the enhancement by the core electrons of the atom of the EFG on the bare nucleus with respect to the EFG due to the outer electron distributions.

The first contribution arises from all ion charges outside the ion under consideration and can be calculated in an approximation assuming point charges,

$$V^{\rm latt}_{\alpha\alpha} = \sum_i \frac{q_i(3\cos^2\theta_i - 1)}{r_i^3}, \tag{11}$$

where q_i is the charge of ion i, located at distance r_i of the probe nucleus in a direction at an angle θ_i from the Z axis of the EFG tensor.

The second term in Eq. (10) arises from unfilled electron shells of the orbitals of the considered site and of the distortions of the inner electron orbitals that they induce, embedded in the known value of $(1 - R_{el})$.

We have then to understand the relative weight of these two contributions in the measured EFG in this particular case of cobaltates. For a fully filled t_{2g} multiplet such as the Co^{3+} low spin state, the ionic structure is isotropic and the second term in Eq. (10) should contribute negligibly to the on site EFG.

Let us then point out that we can deduce significant indications about the respective weights of these two terms by considering the point charge calculations done in Ref. 21. There we deduced average values for the Co1a and Co1b sites of $\nu_Q = 1.32$ MHz and a similar value $\nu_Q \approx 1.48$ MHz for the average of the Co2a and Co2b sites. The corresponding experimental respective values $\nu_Q \approx 1.29$ MHz and $\nu_Q \approx 2.36$ MHz differ significantly. This leads us to suggest then that the excess contribution of about 0.9 MHz on the Co2 sites is due to the on-site hole orbitals. Furthermore, although we cannot rely fully on the numerical values of the point charge calculation, the agreement found with the Co1 data is indeed quite compatible with a negligible contribution of the on-site orbitals on the Co1 sites, that is, with a very small ϵ value.

To check the consistency of this analysis we may compare the data with that obtained for $x = 0.35$, for which we found that the Co sites are uniformly charged.[14] In that case, assuming a simple ordered distribution of Na2 sites and $x = 1/3$, the point charge calculations give values of $\nu_Q \approx 2.5$ MHz for all Co sites, whatever their location with respect to the Na sites, while the NMR data of Ref. 14 correspond to $\nu_Q \simeq 4.1$ MHz. So this much larger value would indicate that a 1.6 MHz on-site contribution should be associated to 2/3 hole per Co site. Such a contribution to ν_Q of 2.4 MHz/hole would correspond to 1.1 MHz for 0.44 holes on the Co2 sites in the $x = 2/3$ phase, remarkably close to the 0.9 MHz value estimated above.

So, although these point charge estimates are certainly not fully reliable, they indicate that the excess EFG found on the Co2 sites has the right order of magnitude and is compatible with the poor hole occupancy of the Co1 sites, as obtained here and above from the analyses of K^{iso} and K^{iso}_{orb}.

C. In-plane anisotropies and orbital order

The simple consideration of the atomic kagome structure displayed in Fig. 11 allows one to expect an asymmetry of the local properties at the Co2 site, and to locate the two orthogonal axes (X^*, Y^*), which should be the Co2 site in-plane local principal axes.

Concerning the electronic structure, it is quite well known that the metallic bands of cobaltates are built from the Co t_{2g} orbitals, which subdivide in the a_{1g} orbital, which is axial and perpendicular to the plane, and two subsets of in plane e'_g orbitals. From LDA calculations of the band structure, done so far for uniformly charged cobaltate planes (see for instance Ref. 38), one usually expected a Fermi surface containing an a_{1g} sheet at the Fermi level centered at the Γ point and e'_g pockets at the zone corners.[5] Only the larger a_{1g} electron pocket has been observed so far by ARPES experiments, whatever the hole content.[39,40] It has often been considered that, even in such simple uniform representations of the CoO_2 plane, the electronic correlations could largely influence the electronic structure by narrowing the bands and possibly pushing the e'_g hole orbitals below the Fermi level.[41]

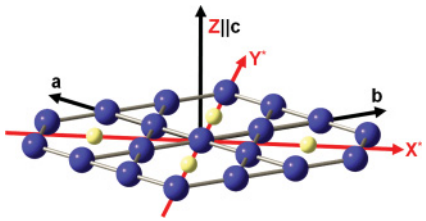

FIG. 11. (Color online) The kagome structure in the CoO_2 planes allows us to clearly locate two orthogonal axes (X^*, Y^*), which should be the Co2 site principal axes in the plane.

All that might not be relevant to the Na ordered and charge disproportionated structures, which would give a smaller Brillouin zone and a larger number of possible bands at the Fermi level. But surprisingly, here we find no experimental sign for multiband behavior. In any case, the dominant magnetic Curie-Weiss behavior is governed by a single band in which correlations are important. So far, the nature of the Co orbitals, which participate in this correlated electronic band, are not readily available from the data. It remains then important to try to determine experimentally what are the respective weights of the a_{1g} and e'_g orbitals involved at the Fermi level in the actual electronic structure of the 2/3 phase.

We consider that the nonaxial NMR parameters determined here may help to answer this question. Assuming that Co1 is in a completely filled-shell Co^{3+} ionic state (that is $\epsilon = 0$), if the electronic structure only results from a_{1g} hole orbitals on the Co2 sites, the nonaxial NMR parameters would only be induced by the absence of transfer integral between Co2 and Co1 sites. But if a fraction of the hole density on Co2 resides on e'_g orbitals, the local asymmetry of the transfer integrals would induce distinct occupancies of the two e'_g orbitals on the Co2 sites. One could expect a larger hole occupancy of the e'_g orbital pointing in the X^* direction in Fig. 11, which would correspond to an ordering of the in-plane hole orbitals on the Co2 sites. In any case, such an unbalanced population of the e'_g orbitals would induce an on-site anisotropy of the NMR parameters on Co2 sites. We shall here try to estimate the a_{1g} and e'_g hole populations by considering first the asymmetry of the EFG and then that of the NMR shifts.

1. In-plane EFG anisotropy on Co2 sites

Both asymmetries of the distributions of Na ions and Co charges located in the plane do introduce an in-plane EFG asymmetry on the Co2 sites. We could evaluate the part of this asymmetry due to ionic charges from the point-charge calculations of the first term of Eq. (10) done in Ref. 21. We, indeed, found that the distribution of Na^+ charges induces a slight tilt of the Z principal axis of the EFG with respect to the c axis on both Co2 sites. The overall ionic charge distribution also results in X and Y principal axes of the EFG, which are

distinct on the Co2a and Co2b sites and which were found markedly modified if we displace the Na atoms with respect to their ideal positions as suggested by the x-ray Rietveldt data analysis of Ref. 21. However, in all cases considered, the computed values of $|V_{YY} - V_{XX}|$ were found to correspond to a difference of NQR frequencies $(\nu_Y - \nu_X)$ in a range between 0.4 and 0.9 MHz. This appears on the average significantly smaller than the 0.8 and 0.9 MHz values deduced from the experimental asymmetry parameter $\eta \approx 0.35$ found for both Co2a and Co2b sites (see Table I).

We may then suggest that some of the nonaxial charge distribution is linked with the on-site term. As the a_{1g} orbital is axial, any on-site nonaxial contribution to the EFG of the Co2 could only result from an unbalance in the populations of the e'_g orbitals.[42,43] The fact that the asymmetry parameter and EFG on the two Co2 sites are quite similar further supports the existence of a sizable on-site e'_g hole-orbital contribution to the EFG. Unfortunately, the large sensitivity of the point-charge calculations of the EFG to the actual atomic structure does not allow us to subtract reliably this EFG contribution from the experimental data, and to deduce then the principal axes and magnitude of the on-site contribution to the EFG. It is clear then that more accurate EFG determinations based on *ab initio* band calculations are needed to relate the EFG data to the relative populations of the a_{1g} and e'_g orbitals.

2. *In-plane Knight shift anisotropies*

While the anisotropy of Na charge distribution contributes to the EFG anisotropy, the Na ions are not involved directly in the magnetic properties, which are fully associated with the CoO_2 layers. So, the anisotropies of the NMR shifts of the Co2 sites should give much better indications on the anisotropy of the in-plane electronic structure. The nonaxial values of the Co2 shifts summarized in Table II are indeed pointing out the existence of an inplane electronic anisotropy. One can notice there that both $K^{\rm orb}$ and $K^{\rm spin}(T)$ are much larger in the X direction than in the Y direction. Let us note that these experimental directions are those identified from the EFG tensor, with the usual convention $|V_{YY}| > |V_{XX}|$, so that the smallest quadrupole frequency occurs in the planar direction for which the NMR shifts are largest, as seen directly in the spectra. However, so far, we do not know for sure how (X,Y) relate to the (X^*,Y^*) axes defined in Fig. 11.

We did find as well an anisotropy of the spin contributions to $(TT_1)^{-1}$ that correlates with the anisotropy of hyperfine couplings, so that no really new information is embedded in this result, especially on the in-plane anisotropy.

a. Orbital shift in-plane anisotropy. SQUID data had allowed us to evidence that the macroscopic susceptibility is larger along the ab plane than in the c direction. These data allowed us to establish that the T dependence of the susceptibility, which is determined by the spin contribution $\chi^{\rm spin}(T)$ is nearly isotropic, which has been confirmed as well from ^{23}Na NMR data.[9] So the susceptibility anisotropy is dominated by that of $\chi^{\rm orb}$ and $\chi^{\rm orb}_{ab} > \chi^{\rm orb}_c$ is sufficiently large to be practical to align the single-crystal grains in the applied field at room temperature. But these SQUID data on powder crystallite samples do not give any indication about the in-plane anisotropy of orbital susceptibility. The present NMR data in Table II establishes a planar anisotropy of $\chi^{\rm orb}$ on the Co2 sites, for which $K^{\rm orb}_X > K^{\rm orb}_Y > K^{\rm orb}_Z$.

Let us point out that $K^{\rm orb}$ can be a purely ionic term, as is the case for Co^{3+}, but states at the Fermi level might also give a specific contribution. This is indeed expected as we found such a metallic band orbital contribution to $(T_1T)^{-1}$ for both Co1 and Co2 sites. In fact, $K^{\rm orb}_Z$ is unmodified with respect to that on Co^{3+}, so that the extra contributions found for $K^{\rm orb}_X$ and $K^{\rm orb}_Y$ could be mainly due to such band contributions, as is suggested by the correlation between the spin and orbital in-plane anisotropies found in Table II. One could notice, however, here again, that if the hole orbitals were purely a_{1g}, one would not expect any in-plane anisotropy of $K^{\rm orb}$, so that here again band calculations of $\chi^{\rm orb}_{\alpha\alpha}$ might help to determine the populations of the a_{1g} and e'_g orbitals.

These observations on the Na and Co sites are reminiscent of the respective situations found for the NMR of the ^{89}Y and of the ^{63}Cu nuclei of the CuO_2 planes of the YBCO cuprates. In that case, as for Na NMR here, the ^{89}Y NMR shift, which is only coupled to spin magnetism, was found nearly isotropic,[44] while the anisotropy of orbital shift of ^{63}Cu was due to that of $\chi^{\rm orb}$, though in that case, the orbital contribution due to the $d_{x^2-y^2}$ in-plane hole orbital[45] does not display any anisotropy in the CuO_2 plane.

b. Spin shift in-plane anisotropy. As the spin susceptibility is nearly isotropic from SQUID and Na NMR shift data, the large in-plane anisotropy of the Co2 NMR spin-shift data $K^{\rm spin}_\alpha(T)$ has to be associated with an anisotropy of hyperfine couplings, which are linked with the occupancy of the electronic orbitals involved at the Fermi level.

Further comparison with the cuprates could help us to better understand the in-plane anisotropy of ^{59}Co NMR spin shifts detected here. Quite generally, the spin shift tensor $K^{\rm spin}_{\alpha\alpha}$ is slightly more complicated than indicated in Eq. (5) as the nuclear spins at site i can be coupled both to the on-site magnetism and to that of their j near-neighbor sites, so that

$$K^{\rm spin}_{\alpha\alpha}(i) = A_{\alpha\alpha}\frac{\chi^{\rm spin}_{\alpha\alpha}(i)}{g\mu_B} + \sum_j B_{\alpha\alpha}\frac{\chi^{\rm spin}_{\alpha\alpha}(j)}{g\mu_B}, \qquad (12)$$

where $A_{\alpha\alpha}$ is the anisotropic on-site hyperfine coupling tensor and $B_{\alpha\alpha}$ is the transferred hyperfine coupling through oxygen orbitals with the j nearest neighbors. In YBCO, there is no hole occupancy on the Y site and therefore no on-site hyperfine coupling $A_{\alpha\alpha}$, so that the hyperfine coupling of ^{89}Y to the Cu site magnetism is only due to the transferred $B_{\alpha\alpha}$, which has been found isotropic.[44] On the contrary, the anisotropy of on-site coupling, $A_{\alpha\alpha}$, is responsible for the large measured (c,ab) anisotropy of the ^{63}Cu spin shift. Even in this simple case with a single Cu axial site, it took sometime to understand that a rather large isotropic value of $B_{\alpha\alpha}$ was required to explain the data.[46] Here, we shall benefit of this approach to perform a tentative preliminary analysis of the Co1 and Co2 data summarized in Table II.

For the axial Co1 sites, only a (c,ab) shift anisotropy is detected. If $\epsilon = 0$, then Co1 sites are nonmagnetic Co^{3+} ions that bear no on-site magnetic spin susceptibility. As the Y ions in the cuprates, they would be inert magnetically and would sense the magnetism of the Co2 orbitals only through transferred hyperfine couplings $B_{\alpha\alpha}$ with the Co2 magnetism.

The (c,ab) anisotropy should then be associated with an anisotropy of the coupling $B_{\alpha\alpha}$ of the Co1 with its first Co2 nearest neighbors. A dipolar coupling of Co1 with its six Co2 neighbors would correspond to a larger negative contribution to the shift for $H \parallel c$, contrary to observation. A nonzero ϵ value with a small filling of the a_{1g} hole orbital on the Co1 would better explain the sign of the (c,ab) anisotropy with a maximum shift contribution for $H \parallel c$.

But, of course, the most intriguing experimental information resides in the totally nonaxial spin shift values found here for the Co2 sites, given in Table II. Averaging the data for the Co2a and Co2b sites results in $K_X^{\rm spin}/^{23}K = 18.9$, $K_Y^{\rm spin}/^{23}K = 7.5$, and $K_Z^{\rm spin}/\,^{23}K = 4.9$.

These large anisotropic contributions to the shift might be dominated by on-site hyperfine couplings with the a_{1g} and e'_g orbitals. We can note here again, as for the discussion of the EFG, that the axial symmetry of the a_{1g}, which points along the c axis, would only yield axial shift contributions and would not differentiate X and Y directions, contrary to the e'_g orbitals. So the large difference between K_X and K_Y can only be attributed to the in-plane order of e'_g orbitals associated with the kagome structure. If one considers the transfer integral paths of e'_g orbitals between Co2 neighboring sites, one would be inclined to associate the X direction, with the largest shift value with the direction X^* sketched in Fig. 11.

Let us note, however, that nothing forbids as well to consider here that the $B_{\alpha\alpha}$ term itself is anisotropic. Detailed consideration of the Wannier orbitals constructed for the full atomic structure of this ordered $x = 1/3$ phase could help to explain these measured anisotropies and would allow altogether to determine the relative populations of a_{1g} and e'_g hole orbitals on the Co2 sites at the Fermi level.

VII. CONCLUSION

In this experiment, we have completely determined experimentally the NMR parameters of the four Co sites of the atomic structure of this $Na_{2/3}CoO_2$ phase, which allows us to confirm that its electronic structure differentiates in fact two sites in the CoO_2 plane: Co1 with a charge $3+\epsilon$ and Co2 with a charge $3.44-\epsilon$. The data for the EFG, the orbital NMR shifts, and orbital T_1T are compatible with a hole content at most of $\epsilon \lesssim 0.06$ on the Co1 site as we had already anticipated.

From our NMR data, we confirm as well that a single band dominates the anomalous electronic properties of this phase at the Fermi level. A totally unexpected aspect revealed by these data is the existence of large in-plane anisotropies of the EFG and NMR shifts on the Co2 site. We have shown that this implies that the hole orbitals on those sites are not exclusively on a_{1g} orbitals and that parts of the holes reside in the e'_g in-plane orbitals, which should then play an important role in the delocalization of the holes.

So the single hole band hybridizes those orbitals and the kagome-like electronic structure that we evidenced then displays not only a charge disproportionation between Co1 and Co2 sites, but as well an in-plane charge order of the t_{2g} orbitals on the Co2 sites. Quantum chemistry calculations taking into account the full structure might permit to go beyond the qualitative arguments developed here and should provide quantitative data for the t_{2g} energy levels from the values obtained experimentally for the EFG, hyperfine couplings, and orbital shift parameters.

One would like then to understand the respective roles of the Na order and of the electronic correlations in driving this electronic structure. In principle, LDA calculations including the Na order should allow to understand whether the Na potential is sufficient to shift down the Co1 t_{2g} energy levels and to induce the Co^{3+} filling of the Co1 orbitals. Preliminary calculations along this line seem to indicate that this is not the case and therefore that it is essential to better take into account the electronic interactions.[47] In such a case, the kagome-like organization of the electronic structure would be an intrinsic disproportionation in the Co planes, which would lock the Na order.[48]

Our work evidences that the resulting situation is quite simple in this $Na_{2/3}CoO_2$ phase, and resumes in a simple two-site charge disproportionated CoO_2 plane, which could be introduced in a simplified model. This would allow one to perform then cluster dynamical mean field theory (DMFT) calculations to establish the role of correlations, which are, of course, essential to explain the large Curie-Weiss-like T dependence found for the susceptibility as well as the 2D ferromagnetic correlations deduced from our spin-lattice relaxation data.[10]

In any case, we have shown that the Na_xCoO_2 compounds display stable Na ordered phases in which charge ordered states of the CoO_2 planes occur so that the real atomic structure has much larger two-dimensional unit cells than that of the CoO_2 plane. We might anticipate then that most ARPES experiments, which isolate a specific surface after cleaving, do not sample the electronic properties of the actual three-dimensional ordered state but are affected by the unavoidable Na disorder in such experimental conditions, although in some cases specific local Na orderings have been observed by STM experiments on cleaved surfaces.[49]

An interesting case is that of some misfit cobaltates[50] for which the multilayer structure is obtained by stacking rocksalt structures with CoO_2 planes. In that case, cleaving is done in the middle of the rocksalt structure, as in high-T_c cuprates, and an ARPES experiment[40] has evidenced that in the specific case of $BaBiCoO_2$, the electronic structure displays a reconstruction, which could result from a charge order analogous to that seen in the Na_xCoO_2 phases. Unfortunately in that case, it has so far not been possible to perform NMR experiments allowing to resolve the sites,[51] so that detailed comparisons are not possible.

Finally, we have established here on a specific case, the importance of charge disproportionation and orbital ordering in this compound. No doubt that for all hole dopings for $x > 0.5$, similar effects do occur as diverse Na orderings are anticipated and observed and result in very distinct correlated electronic states.[2,10,12,15] We think that the present NMR studies allow us to reach a very detailed description of such effects in multiorbital transition oxides.

ACKNOWLEDGMENTS

We would like to thank here A. V. Dooglav and T. A. Platova for the stimulations provided by the NQR experiments, J. Bobroff and P. Mendels for their help on the experimental NMR techniques and for constant interest and stimulating

discussions, and A. N. Lavrov for helpful discussions on material properties aspects. We acknowledge as well G. Collin for his initial unvaluable help on sample characterization and x-ray analysis. We benefited from enlightening discussions with M. B. Lepetit and J. Soret about the quantum chemistry of these systems and with F. Lechermann about the EFG and the band structure of the cobaltates.

I. R. M. thanks for partial support of this work the Russian Foundation for Basic Research (Project No. 10-02-01005a), Ministry of Education and Science of the Russian Federation (Project No. 2010-218-01-192 and Theme No. 1.44.11), and Universite Paris-Sud for associate professor visiting positions. This work has been done within the Triangle de la Physique and H. A. thanks its initial funding by ANR Grant Oxyfonda NT05-4 41913.

APPENDIX A: OXYGEN VACANCIES

A recent publication[22] raises issues with our results[19,21] in order to support structural models of the Na cobaltates that this group has been proposing for many years for large x values.

(i) In this paper, the authors suggest that our samples, being synthesized at high T, are not $Na_{2/3}CoO_2$ but rather $Na_{2/3}CoO_{1.98}$. We can hardly discard solely from our NMR data the presence of such a low content of oxygen vacancies. As each Co has six near-neighbor oxygen, only about 6% of the Co would have such near-neighbor vacancies. If those sites would get well-defined NMR shift and EFG, they should be detected either in NMR or NQR. But as soon as some disorder is expected in the corresponding parameters due to long distance interactions between defects, we would not be able to detect them. We may, however, easily exclude that vacancies could induce perturbations beyond their first nearest neighbors. Those would yield a broad background signal involving then a large Co NMR intensity. So, if present, such oxygen vacancies should just play a similar role to that of Na atoms and give delocalized carriers on the kagome structure, independently of the Co1 sites Co^{3+} signal, which are connected with the ordered Na sites. To conclude on that point, there is, so far, no microscopic experimental evidence for the existence of such oxygen vacancies neither in Ref. 22 nor in our NMR/NQR data.

(ii) Beyond this materials research aspect, Shu *et al.* speculate, again without any microscopic evidence, that the Na order in our samples (putatively, $Na_{2/3}CoO_{1.98}$) might be a structure built from a succession of planes with Na trivacancies and Na tetravacancies,[52] which they have proposed for their sample with an assumed composition of $Na_{0.71}CoO_2$.

We claim that this is definitely contradicted by all our former NMR, NQR, and x-ray data[19,21] and by the present ^{59}Co NMR data. It is easy to establish that this structure corresponds to five Na crystallographic sites (with relative intensities 3/6/3/2/3), and eight Co sites (with relative intensities 1/1/1/3/3/3/3/9). This is well beyond the three Na sites we have detected by NMR[9] and the four Co sites we have detected both by NQR[19,21] and here by NMR. Finally, the structure we have proposed from the analysis of our NMR/NQR data in Ref. 19 has been confirmed by the perfect fit obtained with the Rietveldt x-ray data analysis performed on our samples.[21]

So the self-consistency of our data on our $Na_{2/3}CoO_2$ samples cannot be put into question. Whether the structure proposed by Shu *et al.* for their $Na_{0.71}CoO_2$ samples is the actual one remains a question that might be resolved in the future by performing independent NMR/NQR investigations on their samples.

APPENDIX B: CHECK OF THE POWDER ALIGNMENT BY NMR

The alignment of the sodium cobaltates powders is dependent on the microstructure of the grains, so some of our samples were indeed not well oriented. We demonstrate here how we could use the NMR spectra to distinguish poorly oriented samples from well-oriented ones.

In Fig. 12, we show ^{23}Na NMR spectra measured in two samples of $Na_{2/3}CoO_2$ compound. One of them is a well-oriented sample (Sample A), and we show there the spectra measured in two directions of the applied magnetic field: $H_0 \perp c$ and $H_0 \parallel c$. As evidenced before,[9,21] in the $Na_{2/3}CoO_2$ phase, there are three inequivalent sodium sites: Na1, Na2a, and Na2b. We found that although the central lines and satellite singularities of the ^{23}Na spectrum can be easily located, the overall shape of the NMR spectrum is very sensitive to the degree of orientation of the powder sample. In Fig. 12, we also show results of the computer simulations of the ^{23}Na NMR spectra using the parameters of Eq. (2) from Ref. 9. Here, we have optimized the particles c-axis angular-orientation distribution to fit accurately the

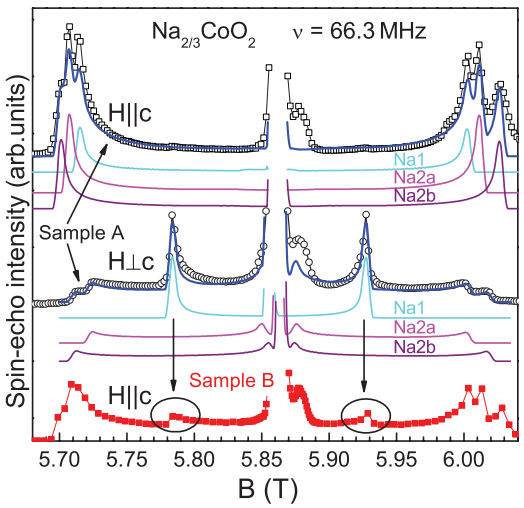

FIG. 12. (Color online) ^{23}Na NMR spectra: comparison of oriented sample A (black open circles for $H_0 \perp c$ and open squares for $H_0 \parallel c$) and sample B (red closed squares for $H_0 \parallel c$). The solid color lines display the computed spectra for the three different Na sites, and the total spectum which fits perfectly the data for sample A. The presence of the Na1 singularities specific for the $H_0 \perp c$ direction spectrum of sample A in the $H_0 \parallel c$ spectrum of sample B is clear and allowed us to conclude that sample A is better oriented than sample B. The extra line near the central transition at about 5.88 T with a small Knight shift has a very weak intensity, which corresponds at most to 5% of all Na nuclei, and might be assigned to defect sites in the ordered Na structure, or to a minute amount of impurity phases present in these samples with large crystallites.

spectrum (Lorentzian distribution of $\pm 5^\circ$ width). It's important to mention that we used exactly the same angular distribution parameters for the ^{59}Co simulations shown in Figs. 3–6. As one can see, the agreement between experimental and simulated spectra is very good.

At the bottom of Fig. 12, we show a ^{23}Na NMR spectrum measured in Sample B of $Na_{2/3}CoO_2$, which happened to be less well oriented. Comparing this spectrum with that measured in Sample A, it is easy to see for $H_0 \parallel c$, the presence of Na1 singularities specific to the $H_0 \perp c$ direction of applied magnetic field. That is due to a fraction of particles, which remained randomly oriented as they were either not single crystallites, or were too much packed or agglomerated and could not orient. Also a less prominent, but still detectable feature of this less-oriented sample, is the poor resolution of the quadrupolar satellites.

In Fig. 13, we demonstrate the distinction between the ^{59}Co NMR spectra measured in these two samples as well. The comparison can be summarized as follows. (1) First of all, in Sample B spectrum, measured for $H_0 \parallel c$, one can see an extra line, circled as (1), which corresponds to the central lines of Co1a and Co1b sites in the $H_0 \perp c$ direction (marked by arrow in Fig. 13). (2) Also one can see that for the well-oriented Sample A, the NMR spectrum measured for $H_0 \parallel c$ is rather symmetric, whereas the spectrum for $H_0 \perp c$ is asymmetric with a higher signal intensity for the lower field values, which could be assigned to fast relaxing cobalts. In Sample B, even in the $H_0 \parallel c$ spectrum, some asymmetry could be seen and is here again associated with the contribution from grains, which did not orient in the field. This extra intensity, circled as (2), had misled us by suggesting that a Co site labeled as Co3 could have a large purely axial shift [see Fig. 2(c) in Ref. 3]. Again in the sample B spectrum, the quadrupolar satellites are less resolved as one can see in Fig. 13, on the part circled as (3).

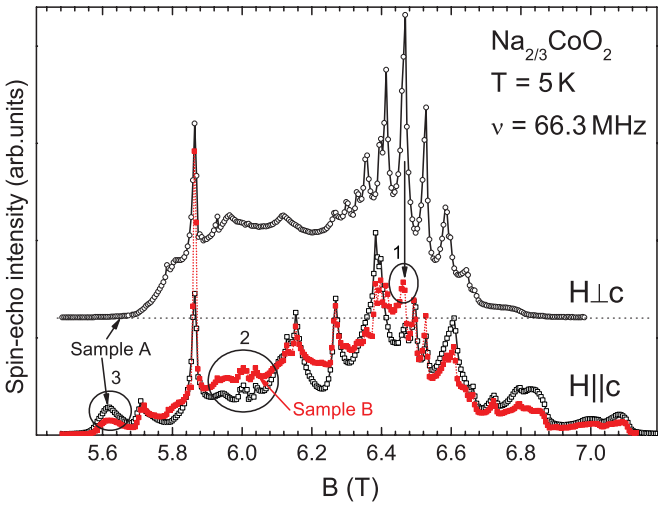

FIG. 13. (Color online) Comparison of ^{59}Co NMR spectra of the well oriented sample A (black open circles for $H_0 \perp c$ and open squares for $H_0 \parallel c$) with that of the less well-oriented sample B (red closed squares for $H_0 \parallel c$). The extra contributions in the $H_0 \parallel c$ spectrum of sample B due to the Co1 and Co2 signals of nonoriented particles are highlighted within circles (1) and (2).

APPENDIX C: DETERMINATION OF $K(T)$ FROM FULL ANALYSES OF THE ^{59}Co NMR SPECTRA

The ^{59}Co NMR of the slow relaxing Co1 sites in the $Na_{\approx 0.7}CoO_2$ compounds are easy to observe and were seen even by continuous-wave NMR.[53] In the $Na_{2/3}CoO_2$ compound, even small details for the Co1a and Co1b sites could be detected and have been reported.[31] The axial symmetry of these sites symmetrizes the magnetic shift and quadrupolar tensors, which makes the NMR lines of ^{59}Co in these positions rather narrow and intense.

The case is more complicated for the fast-relaxing Co2 sites in the $Na_{\approx 0.7}CoO_2$ compounds. Even in the single crystals, the NMR spectra of these sites are broad and not well resolved.[23] The same situation occurs in our oriented powder samples; see Fig. 2 as an example. As in our samples, the c axis of different crystallites are aligned along $H_0 \parallel c$ and one can distinguish in the spectrum the two sets of seven lines, which correspond to the different transitions $m \leftrightarrow (m-1)$ for the two cobalt sites Co2a and Co2b. For $H_0 \perp c$, the NMR spectrum of the fast-relaxing cobalts is found broad and nonresolved, as the particles in our samples have a powder distribution of ab axes for $H_0 \perp c$. This experimental fact immediately tells that the local symmetry for the Co2 sites is lower than for the Co1 sites.

To clarify the spectra of the Co2 sites for $H_0 \perp c$, we used various facts: (1) the position of the different singularities in the fast-relaxing Co2 spectra are the same whatever the sample and whatever the sample preparation method, as one can see in Fig. 2. The positions of the singularities in the NMR spectra depend on both the quadrupole splitting (which could be considered practically as temperature independent) and the magnetic shift, which scales with the susceptibility $\chi_s(T)$. (2) The main feature of the $Na_{2/3}CoO_2$ phase is a large temperature dependence of the spin susceptibility. As we have shown, the local fields are quite similar for the three detected Na sites,[9] the first moment (center of gravity) of the ^{23}Na NMR spectrum $^{23}K_s^{\rm iso} = A\chi_s(T)$ allows us to follow the spin susceptibility $\chi_s(T)$ of the cobalts up to room T. Therefore using $^{23}K_s^{\rm iso}(T)$ as a reference, we tried to follow the corresponding T variation of the Co shift tensor.

We measured then the ^{59}Co NMR spectra at different temperatures in swept field mode and at each temperature pointed the positions (field values) of all singularities in the spectra of fast-relaxing Co2. After that, we converted them into field shift values using Eq. (4) and plotted them versus $^{23}K(T)$ taken at the measurement temperature. Each spectrum taken at a given T then allows to report all the data points on a vertical line in Fig. 14(a).

As one can see, some singularities for the fast-relaxing Co2 appear well organized around extremal values of the shift, with $3+3$ satellites spaced by the quadrupole splitting ν_α; in Fig. 14(b), we show two such sets of singularities by lines. Initially, we assumed that these two sets of singularities correspond to the two cobalt sites: one with a large shift in $H_0 \perp c$ direction and the other a small shift, but this assumption did not allow us to explain all the data.

Unexpectedly, we found that the values of quadrupole splitting ν_α for these two sets of singularities correspond to the ν_X and ν_Y values of the Co2b site (the corresponding ν_Q

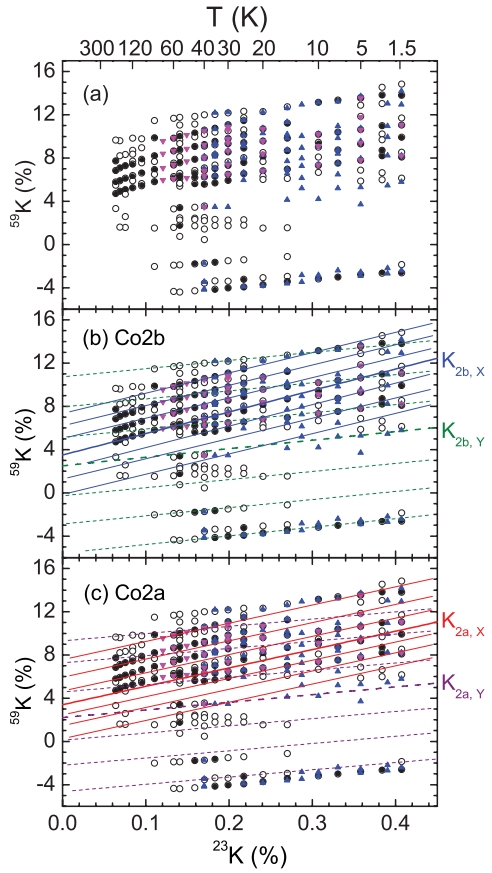

FIG. 14. (Color online) (a) The global summary of all our magnetic shift data for the various singularities of the fast-relaxing cobalt spectra, plotted vs the isotropic component of the ^{23}Na NMR shift. The most pronounced singularities in the experimental spectra are marked by filled symbols, whereas weaker singularities are displayed with open symbols. Different symbols correspond to spectra for differently prepared samples of the same phase. (b) Here, the same data are reported, but with lines drawn that underline the central line and six quadrupolar satellites of ^{59}Co in the Co2b positions for $H_0 \parallel X$ (blue full lines) and $H_0 \parallel Y$ (green dashed lines) directions. (c) On the same data again, we have drawn the seven ^{59}Co NMR lines, which correspond to the Co2a positions for $H_0 \parallel X$ (red full lines) and $H_0 \parallel Y$ (magenta dashed lines) directions.

and η values were determined by NQR with high presicion).[21] Therefore the main conclusion of Fig. 14(b) is that we have

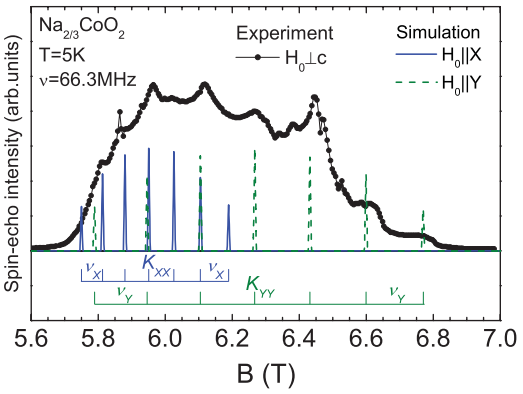

FIG. 15. (Color online) The ^{59}Co NMR spectrum of fast-relaxing Co2 is shown by full dots joined by a continuous line. The positions of the seven lines estimated from the full data analysis are shown for $H_0 \parallel X$ (blue solid line) and $H_0 \parallel Y$ (green dashed line). The correspondence with the singularities in the experimental spectrum is clear. The position of these two sets of singularities is then determined by these extremal lines, while most of the intensity in the spectrum comes from the particles with intermediate orientations. The large singularities around 6.4 T comes from imperfect compensation of the large signal of the slow-relaxing Co1 sites.

a large anisotropy of in-plane magnetic shift for the dominant Co2b site with distinct values of K_{XX} and K_{YY}.

As the number of Co2a sites in the unit cell of the $Na_{2/3}CoO_2$ phase is twice smaller than that of Co2b sites, the intensity of their NMR signal is also twice smaller. This makes more difficult to resolve the Co2a site in the $H_0 \perp c$ spectra. As one can see in Fig. 14(b), many singularities are located in between the identified Co2b singularities. Using them and the values of ν_Q and η for Co2a sites,[21] one can suggest two sets of singularities for the Co2a sites [see Fig. 14(c)]. And in fact, the Co2a sites exhibit the same in-plane magnetic shift anisotropy as the Co2b sites, just with slightly smaller values of the magnetic shifts and quadrupole splittings.

Therefore the fast-relaxing cobalt $H_0 \perp c$ spectra can be finally explained in a simple manner. In Fig. 15, we show the simulated set of NMR lines of Co2b for the two outermost cases for which $H_0 \parallel X$ and $H_0 \parallel Y$. These two spectra form the main singularities in the cobalt spectra while most of its intensity comes from the particles with intermediate orientations. The large difference in the K_{XX} and K_{YY} values makes the cobalt $H_0 \perp c$ spectra totally asymmetric.

*irek.mukhamedshin@ksu.ru

[1] I. Terasaki, Y. Sasago, and K. Uchinokura, Phys. Rev. B **56**, R12685 (1997).
[2] P. Mendels, D. Bono, J. Bobroff, G. Collin, D. Colson, N. Blanchard, H. Alloul, I. Mukhamedshin, F. Bert, A. Amato, and A. D. Hillier, Phys. Rev. Lett. **94**, 136403 (2005).
[3] M. L. Foo, Y. Wang, S. Watauchi, H. W. Zandbergen, T. He, R. J. Cava, and N. P. Ong, Phys. Rev. Lett. **92**, 247001 (2004).
[4] K. Takada, H. Sakurai, E. Takayama-Muromachi, F. Izumi, R. A. Dilanian, and T. Sasaki, Nature (London) **422**, 53 (2003).
[5] D. J. Singh, Phys. Rev. B **61**, 13397 (2000).
[6] P. Abbamonte, A. Rusydi, S. Smadici, G. D. Gu, G. A. Sawatzky, and D. L. Feng, Nature (London) Physics **1**, 155 (2005).
[7] Y. Ando, K. Segawa, S. Komiya, and A. N. Lavrov, Phys. Rev. Lett. **88**, 137005 (2002).
[8] H. W. Zandbergen, M. L. Foo, Q. Xu, V. Kumar, and R. J. Cava, Phys. Rev. B **70**, 024101 (2004).
[9] I. R. Mukhamedshin, H. Alloul, G. Collin, and N. Blanchard, Phys. Rev. Lett. **93**, 167601 (2004).

[10]H. Alloul, I. R. Mukhamedshin, G. Collin, and N. Blanchard, Europhys. Lett. **82**, 17002 (2008).
[11]M. Roger, D. J. P. Morris, D. A. Tennant, M. J. Gutmann, J. P. Goff, J.-U. Hoffmann, R. Feyerherm, E. Dudzik, D. Prabhakaran, A. T. Boothroyd, N. Shannon, B. Lake, and P. P. Deen, Nature (London) **445**, 631 (2006).
[12]G. J. Shu, A. Prodi, S. Y. Chu, Y. S. Lee, H. S. Sheu, and F. C. Chou, Phys. Rev. B **76**, 184115 (2007).
[13]F.-T. Huang, M.-W. Chu, G. J. Shu, H. S. Sheu, C. H. Chen, L.-K. Liu, P. A. Lee, and F. C. Chou, Phys. Rev. B **79**, 014413 (2009).
[14]I. R. Mukhamedshin, H. Alloul, G. Collin, and N. Blanchard, Phys. Rev. Lett. **94**, 247602 (2005).
[15]G. Lang, J. Bobroff, H. Alloul, G. Collin, and N. Blanchard, Phys. Rev. B **78**, 155116 (2008).
[16]M.-H. Julien, C. de Vaulx, H. Mayaffre, C. Berthier, M. Horvatić, V. Simonet, J. Wooldridge, G. Balakrishnan, M. R. Lees, D. P. Chen, C. T. Lin, and P. Lejay, Phys. Rev. Lett. **100**, 096405 (2008).
[17]J. Bobroff, G. Lang, H. Alloul, N. Blanchard, and G. Collin, Phys. Rev. Lett. **96**, 107201 (2006).
[18]F. L. Ning, S. M. Golin, K. Ahilan, T. Imai, G. J. Shu, and F. C. Chou, Phys. Rev. Lett. **100**, 086405 (2008).
[19]H. Alloul, I. R. Mukhamedshin, T. A. Platova, and A. V. Dooglav, Europhys. Lett. **85**, 47006 (2009).
[20]Y. Hinuma, Y. S. Meng, and G. Ceder, Phys. Rev. B **77**, 224111 (2008).
[21]T. A. Platova, I. R. Mukhamedshin, H. Alloul, A. V. Dooglav, and G. Collin, Phys. Rev. B **80**, 224106 (2009).
[22]G. J. Shu, W. L. Lee, F.-T. Huang, M.-W. Chu, P. A. Lee, and F. C. Chou, Phys. Rev. B **82**, 054106 (2010).
[23]F. L. Ning, T. Imai, B. W. Statt, and F. C. Chou, Phys. Rev. Lett. **93**, 237201 (2004).
[24]Y. Wang, N. S. Rogado, R. J. Cava, and N. P. Ong, Nature (London) **423**, 425 (2003).
[25]A. Egorov, O. Bakharev, A. Volodin, S. Korableva, M. Tagirov, and M. Teplov, Sov. Phys. JETP **70**, 658 (1990).
[26]T. A. Platova, I. R. Mukhamedshin, A. V. Dooglav, and H. Alloul, JETP Lett. **91**, 421 (2010).
[27]A. Abragam, *The Principles of Nuclear Magnetism* (Oxford: Clarendon Press, London, 1961).
[28]C. P. Slichter, *Principles of Magnetic Resonance*, 3rd ed. (Springer-Verlag, Berlin, New York, 1990).
[29]A. V. Egorov, I. R. Mukhamedshin, and H. Suzuki, Physica B: Condensed Matter **329–333**, 1397 (2003).
[30]Y. Ihara, K. Ishida, C. Michioka, M. Kato, K. Yoshimura, H. Sakurai, and E. Takayama-Muromachi, J. Phys. Soc. Jpn. **73**, 2963 (2004).
[31]J. L. Gavilano, B. Pedrini, K. Magishi, J. Hinderer, M. Weller, H. R. Ott, S. M. Kazakov, and J. Karpinski, Phys. Rev. B **74**, 064410 (2006).
[32]T. Moriya, J. Phys. Soc. Jpn. **18**, 516 (1963).
[33]E. Andrew and D. Tunstall, Proc. Phys. Soc. **78**, 1 (1961).
[34]A. F. Mcdowell, J. Magn. Reson., Ser. A **113**, 242 (1995).
[35]Y. Obata, J. Phys. Soc. Jpn. **18**, 1020 (1963).
[36]G. Lang, J. Bobroff, H. Alloul, P. Mendels, N. Blanchard, and G. Collin, Phys. Rev. B **72**, 094404 (2005).
[37]C. de Vaulx, M.-H. Julien, C. Berthier, M. Horvatić, P. Bordet, V. Simonet, D. P. Chen, and C. T. Lin, Phys. Rev. Lett. **95**, 186405 (2005).
[38]D. Pillay, M. D. Johannes, I. I. Mazin, and O. K. Andersen, Phys. Rev. B **78**, 012501 (2008).
[39]H.-B. Yang, Z.-H. Pan, A. K. P. Sekharan, T. Sato, S. Souma, T. Takahashi, R. Jin, B. C. Sales, D. Mandrus, A. V. Fedorov, Z. Wang, and H. Ding, Phys. Rev. Lett. **95**, 146401 (2005).
[40]A. Nicolaou, V. Brouet, M. Zacchigna, I. Vobornik, A. Tejeda, A. Taleb-Ibrahimi, P. L. Fvre, F. Bertran, C. Chambon, S. Kubsky, S. Hbert, H. Muguerra, and D. Grebille, Europhys. Lett. **89**, 37010 (2010).
[41]A. Liebsch and H. Ishida, Eur. Phys. J. B **61**, 405 (2008).
[42]M. B. Lepetit (private communication).
[43]J. Soret, PhD. thesis, Université de Caen, Basse-Normandie, France (2010).
[44]H. Alloul, A. Mahajan, H. Casalta, and O. Klein, Phys. Rev. Lett. **70**, 1171 (1993).
[45]M. Takigawa, P. C. Hammel, R. H. Heffner, and Z. Fisk, Phys. Rev. B **39**, 7371 (1989).
[46]F. Mila and T. Rice, Physica C: Superconductivity **157**, 561 (1989).
[47]F. Lechermann (private communication).
[48]L. Boehnke and F. Lechermann, e-print arXiv:1012.5943 (unpublished).
[49]W. W. Pai, S. H. Huang, Y. S. Meng, Y. C. Chao, C. H. Lin, H. L. Liu, and F. C. Chou, Phys. Rev. Lett. **100**, 206404 (2008).
[50]A. Maignan, S. Hebert, M. Hervieu, C. Michel, D. Pelloquin, and D. Khomskii, J. Phys. Condens. Matter **15**, 2711 (2003).
[51]J. Bobroff, S. Hébert, G. Lang, P. Mendels, D. Pelloquin, and A. Maignan, Phys. Rev. B **76**, 100407 (2007).
[52]G. J. Shu, F.-T. Huang, M.-W. Chu, J.-Y. Lin, P. A. Lee, and F. C. Chou, Phys. Rev. B **80**, 014117 (2009).
[53]R. Ray, A. Ghoshray, K. Ghoshray, and S. Nakamura, Phys. Rev. B **59**, 9454 (1999).